43 p.

NASA TECHNICAL NOTE

NASA TN D-1958

N63 21891
CODE-1

NASA TN D-1958

TRANSONIC WIND-TUNNEL INVESTIGATION OF THE STATIC AERODYNAMIC CHARACTERISTICS OF SEVERAL CONFIGURATIONS OF THE BLUE SCOUT LAUNCH VEHICLE

by Thomas C. Kelly and Robert J. Keynton;
Langley Research Center,
Langley Station, Hampton, Va.

NATIONAL AERONAUTICS AND SPACE ADMINISTRATION - WASHINGTON, D. C. - SEPTEMBER 1963

TECHNICAL NOTE D-1958

TRANSONIC WIND-TUNNEL INVESTIGATION OF THE STATIC AERODYNAMIC CHARACTERISTICS OF SEVERAL CONFIGURATIONS OF THE BLUE SCOUT LAUNCH VEHICLE

By Thomas C. Kelly and Robert J. Keynton

Langley Research Center
Langley Station, Hampton, Va.

NATIONAL AERONAUTICS AND SPACE ADMINISTRATION

NATIONAL AERONAUTICS AND SPACE ADMINISTRATION

TECHNICAL NOTE D-1958

TRANSONIC WIND-TUNNEL INVESTIGATION OF THE STATIC AERODYNAMIC CHARACTERISTICS OF SEVERAL CONFIGURATIONS OF THE BLUE SCOUT LAUNCH VEHICLE

By Thomas C. Kelly and Robert J. Keynton

SUMMARY

Results have been obtained in the Langley 8-foot transonic pressure tunnel at Mach numbers from 0.60 to 1.03 for several variations of a 1/15-scale model of the Blue Scout and the basic Blue Scout 609A configuration. The investigation extended over angle-of-attack and sideslip ranges from about -6° to 6° at a Reynolds number per foot of approximately 3.7×10^6.

Results indicate that for a configuration having no fins, the addition of base flares results in sizable increases in normal-force-curve slope near an angle of attack of 0°, which are accompanied by rearward shifts in center-of-pressure location. For the finned configuration, the addition of the base flares had only slight effects as a result of a sizable portion of the fin being covered by the flare. Addition of protuberances (antennas, wiring conduits, and launch fitting) to the basic configuration resulted in a slight forward shift in center-of-pressure location primarily due to the addition of flat-plate antennas which were mounted near the forward end of the vehicle and which act, in effect, as small low-aspect-ratio canard surfaces.

INTRODUCTION

The development of the NASA Scout launch vehicle has been accompanied by the parallel development, by the U.S. Air Force, of the Blue Scout 609A family of vehicles. The four-stage Blue Scout is generally similar to the basic NASA Scout and utilizes many of the NASA Scout components. The Blue Scout has the capability of performing orbital, reentry, and deep space probe missions, and was developed to allow the use of payloads of increased volume relative to those of the basic Scout vehicle.

As part of the vehicle development program, tests have been conducted in the Langley 8-foot transonic pressure tunnel at Mach numbers from 0.60 to 1.03 and at angles of attack and sideslip from about -6° to 6° to determine the static aerodynamic characteristics for a 1/15-scale model of the four-stage Blue Scout.

Included in the investigation was the determination of the effects of fins, protuberances (antennas, wiring conduits, and launch fitting), first-stage base flare angle, and, for the basic configuration, fin-tip control deflection. Results of tests of other Scout, Blue Scout, and related configurations are available in references 1 to 7.

SYMBOLS

Aerodynamic force and moment data are referred to the body system of axes, with coefficients based on an area of 0.0388 square foot and a length of 2.668 inches which correspond to the model maximum cylindrical cross-sectional area and diameter, respectively. Moments are measured about a point located at 66.3 percent of the overall model length (measured from the theoretical nose-cone apex to the fin trailing edge).

A body maximum cross-sectional area, sq ft

C_A axial-force coefficient, $\frac{\text{Axial force}}{qA}$

$C_{A,b}$ base axial-force coefficient, $\frac{\text{Base axial force}}{qA}$

C_l rolling-moment coefficient, $\frac{\text{Rolling moment}}{qAd}$

C_{l_β} change in rolling-moment coefficient due to sideslip, per degree

C_m pitching-moment coefficient, $\frac{\text{Pitching moment}}{qAd}$

C_{m_α} pitching-moment-curve slope, $\frac{\partial C_m}{\partial \alpha}$, per degree (measured at $\alpha = 0^\circ$)

C_N normal-force coefficient, $\frac{\text{Normal force}}{qA}$

C_{N_α} normal-force-curve slope, $\frac{\partial C_N}{\partial \alpha}$, per degree (measured at $\alpha = 0^\circ$)

C_n yawing-moment coefficient, $\frac{\text{Yawing moment}}{qAd}$

C_{n_β} change in yawing-moment coefficient due to sideslip, per degree

C_Y side-force coefficient, $\frac{\text{Side force}}{qA}$

C_{Y_β} change in side-force coefficient due to sideslip, per degree

d body maximum cylindrical diameter, in.

l model overall length, measured from nose-cone apex to fin trailing edge, in.

M Mach number

q free-stream dynamic pressure, lb/sq ft

R Reynolds number per foot

r radius of curvature

x distance, measured from nose-cone apex, in.

α angle of attack of body center line, deg

β angle of sideslip of body center line, deg

δ_f first-stage base flare half-angle, deg

δ_t fin tip-control deflection angle, deg

Subscript:

cp center of pressure

APPARATUS AND TESTS

Models

Details and design dimensions for the 1/15-scale model of the basic Blue Scout configuration are presented in figure 1(a). The cruciform fins, mounted with the trailing edge slightly rearward of the first-stage base, have a leading-edge sweepback of 45° and employ single-wedge airfoil sections having a streamwise included angle of 8°. The fin leading edges were blunted and had a radius of curvature (measured normal to the leading edge) of 0.017 inch. Details of the flat-plate antennas and the wiring conduits are shown in figure 1.

Several model configurations were tested both with and without fins (see fig. 1(b)), and are described as follows:

Configuration	Description
A	Body alone (no base flare)
B	Body with 13.5° base flare
C	Body with 16.0° base flare
D	Body with fins (no base flare)
E	Body with fins and 13.5° base flare
F	Body with fins and 16.0° base flare
G	Body, fins, 13.5° base flare, with antennas, wiring conduits, and launch fitting (basic configuration)
H	Body, fins, 13.5° base flare, antennas, conduits, and launch fitting with 4 fin-tip controls at $\delta_t = 10°$
I	Body, fins, 13.5° base flare, with conduits and launch fitting (antennas off)

Photographs of the basic configuration are presented in figure 2. It should be noted that in the photographs the model has been rolled 90° and is shown with the top facing the viewer.

Tests and Procedure

Tests were conducted in the Langley 8-foot transonic pressure tunnel over a Mach number range from 0.60 to 1.03 and through angle-of-attack and sideslip ranges from approximately -6° to 6°. Reynolds numbers per foot varied from about 3.18×10^6 at a Mach number of 0.60 to 4.12×10^6 at a Mach number of 1.03. (See fig. 3.)

All tests were conducted with transition fixed at a location 3.56 inches rearward of the nose-cone apex. The transition strip was 0.1 inch wide and was composed of No. 80 carborundum grains set in a plastic adhesive.

Corrections

Effects of subsonic boundary interference in the slotted test section are considered negligible and no corrections for these effects have been applied. At supersonic speeds, the data are generally affected by boundary-reflected disturbances which occur at Mach numbers from slightly over 1.03 to those at which the disturbances are reflected downstream of the model base. For the present tests, the model length and tunnel power restrictions precluded the attainment of a Mach number at which the model would be reflection free. Therefore, no results are presented for Mach numbers higher than 1.03.

Axial-force data have been adjusted to correspond to the condition of free-stream static pressure acting at the model and flare bases.

PRESENTATION OF RESULTS

In order to facilitate presentation of the data, staggered scales have been used in some of the figures and care should be taken in selecting the proper zero axis for each curve. Center-of-pressure results (presented in figs. 7, 8, and 12) are based on the model overall length from the theoretical nose-cone apex to the fin trailing edge. The flagged points which appear at angles of attack and sideslip of 0° represent computed values which were obtained by using C_{m_α} and C_{N_α} (or C_{n_β} and C_{Y_β}) measured at an angle of attack (or sideslip) of approximately 0°. A list of figures presenting results of this investigation is given below:

RESULTS AND DISCUSSION

Longitudinal Characteristics

Effects of base flares and fins.- Results showing the effects of base flares and fins on the aerodynamic characteristics in pitch are presented in figures 4 to 7 and are summarized in figure 8. These results are qualitatively similar to those presented in reference 3 in that addition of a base flare to the body without fins causes a substantial increase in normal-force-curve slope at angles of attack near 0° whereas addition of the same flare to the body with fins attached generally causes only slight increases in the slope of the normal-force curve. (See figs. 4(a), 4(b), and 8(a).) As an example, results presented in figure 8(a) show that at a Mach number of 0.8, addition of the 13.5° flare to the body with no fins increases C_{N_α} from 0.050 to 0.104 or by 0.054. Addition of the same flare to the body with fins causes an increase in C_{N_α} from 0.184 to 0.192, or by 0.008. At the higher Mach numbers, the increment in C_{N_α} due to adding the flare to the body with no fins remains about equal to the value noted for a Mach number of 0.80 but for the finned configuration little or no gain in C_{N_α} is seen to result from the flare addition.

Results corresponding to those noted above are also evident in the pitching-moment and center-of-pressure characteristics for the various configurations. Results presented in figure 8(a) indicate a rearward shift in center of pressure of about 38 percent of the body length due to addition of the flares to the configuration with no fins. For the finned configuration, addition of the flares had little or no effect on the center-of-pressure location. The primary reason for the variations noted, as was mentioned for similar configurations in reference 3, is that in the process of adding a base flare to the finned configuration, a sizable portion of the delta planform fin is covered by the flare and results in a loss in fin lift. Also, because of the fin-flare arrangement for the present configuration, a portion of the fin immediately behind the flare base is "blanketed" by the flare wake and probably carries little or no lift. The flare and wake coverage (for the basic 13.5° flare configuration) amounts to about 33 percent of the total fin area. These flare effects, as noted earlier, apply to the angle-of-attack range near 0°. As angle of attack is increased, C_{N_α} generally decreases for the flared configurations (fig. 4) and C_{m_α} increases by a relatively greater degree (fig. 6). This increase in C_{m_α} results in a forward shift in center-of-pressure location, the magnitude of which increases with an increase in Mach number. (See fig. 7.) The effects are more pronounced for the flared configurations having no fins. (Compare figs. 7(a) and 7(b).)

Axial-force results, presented in figure 8(c), indicate expected variations in that the addition of flares to the configurations with or without fins results in increases in the axial-force and base axial-force coefficients and in the transonic drag rise. Similarly, the addition of fins to the configurations with or without flares has noticeable effects on the axial-force coefficients and on the drag rise, and somewhat lesser effects on the base axial-force coefficients.

Effects of protuberances, basic configuration.- The effects of adding protuberances (antennas, wiring conduits, and launch fitting) to the basic configuration (13.5° base flare) may be noted by comparing configurations E and G in figures 4 to 7. A summary of these results, given in figure 8, indicates the effects on the aerodynamic characteristics are generally slight. It is interesting to note that for Mach numbers near 1.0, the addition of protuberances results in a slight decrease in stability and forward center-of-pressure shift (fig. 8(b)). This result is apparently associated with the flat-plate antennas which act, in effect, as extremely small low-aspect-ratio canard surfaces which are mounted well forward on the vehicle. (Compare configurations G and I in figs. 6(c), 7(c), and 8(b).)

Lateral Characteristics

Effects of protuberances, basic configuration.- Results showing the effects of protuberances on the lateral aerodynamic characteristics for the basic configuration G are presented in figures 9 to 12. Examination of figures 10(a) and 12(a) indicates that, as a result of the larger planform antennas installed in the vertical plane, the forward shift in center of pressure resulting from the addition of the antennas is more apparent over a greater Mach number range than was the case for the horizontally oriented antennas.

Of interest also are the variations of C_l, C_n, and C_Y with angle of sideslip at an angle of attack of 5°. Rolling-moment results, presented in figure 9(b), indicate negative effective dihedral $\left(+C_{l_\beta}\right)$ for the configurations shown at all Mach numbers near an angle of sideslip of 0°. Yawing-moment results (fig. 10(b)) show sizable individual effects of both the antennas and the remaining protuberances, and side-force variations (fig. 11(b)) indicate noticeable effects of the antennas, particularly at the highest test Mach numbers, and random effects due to the other protuberances.

Effects of tip control deflection.- The effects of deflecting the four tip controls 10°, shown in figure 13, are seen to result in an increment in rolling-moment coefficient of about 0.15, the magnitude remaining fairly constant with variations in either angle of attack or Mach number.

CONCLUDING REMARKS

Results of an investigation of several configurations of a 1/15-scale model of the Blue Scout 609A vehicle have indicated the following:

For the configuration having no fins, the addition of base flares results in sizable increases in normal-force-curve slope near an angle of attack of 0°, accompanied by rearward shifts in center-of-pressure location. For the finned configuration, the addition of the base flares had only slight effects as a result of a sizable portion of the fin being covered by the flare. Addition of protuberances (antennas, wiring conduits, and launch fitting) resulted in slight forward shifts in center-of-pressure location at Mach numbers near 1.0 primarily due to the addition of flat-plate antennas which were mounted near the forward end of the vehicle and which act, in effect, as small low-aspect-ratio canard surfaces.

Langley Research Center,
National Aeronautics and Space Administration,
Langley Station, Hampton, Va., June 17, 1963.

REFERENCES

1. Jernell, Lloyd S., and Wong, Norman: Investigation of the Static Longitudinal Stability Characteristics of a 0.067-Scale Model of a Four-Stage Configuration of the Scout Research Vehicle at Mach Numbers of 2.29, 2.96, 3.96, and 4.65. NASA TN D-554, 1960.

2. Robinson, Ross B.: Aerodynamic Characteristics in Pitch and Sideslip of a 1/15-Scale Model of the Scout Vehicle at a Mach Number of 2.01. NASA TN D-793, 1961.

3. Kelly, Thomas C.: Transonic Wind-Tunnel Investigation of the Static Longitudinal Aerodynamic Characteristics of Several Configurations of the Scout Vehicle and of a Number of Related Models. NASA TN D-794, 1961.

4. Keynton, Robert J., and Fichter, Ann B.: Investigation of the Aerodynamic Characteristics of Two Preliminary Designs of Scout Research Vehicle at Mach Numbers From 1.77 to 4.65. NASA TN D-821, 1961.

5. Kelly, Thomas C.: Aerodynamic Loading Characteristics at Mach Numbers From 0.80 to 1.20 of a 1/10-Scale Three-Stage Scout Model. NASA TN D-945, 1961.

6. Kelly, Thomas C., and Keynton, Robert J.: Investigation of the Static Longitudinal Aerodynamic Characteristics of a 1/10-Scale Model of the Blue Scout Jr. at Mach Numbers From 0.40 to 1.03. NASA TN D-1228, 1962.

7. Jernell, Lloyd S.: Static Stability Characteristics of Models of the Blue Scout and the Blue Scout, Jr., Research Vehicles at Mach Numbers From 2.29 to 3.75. NASA TN D-1931, 1963.

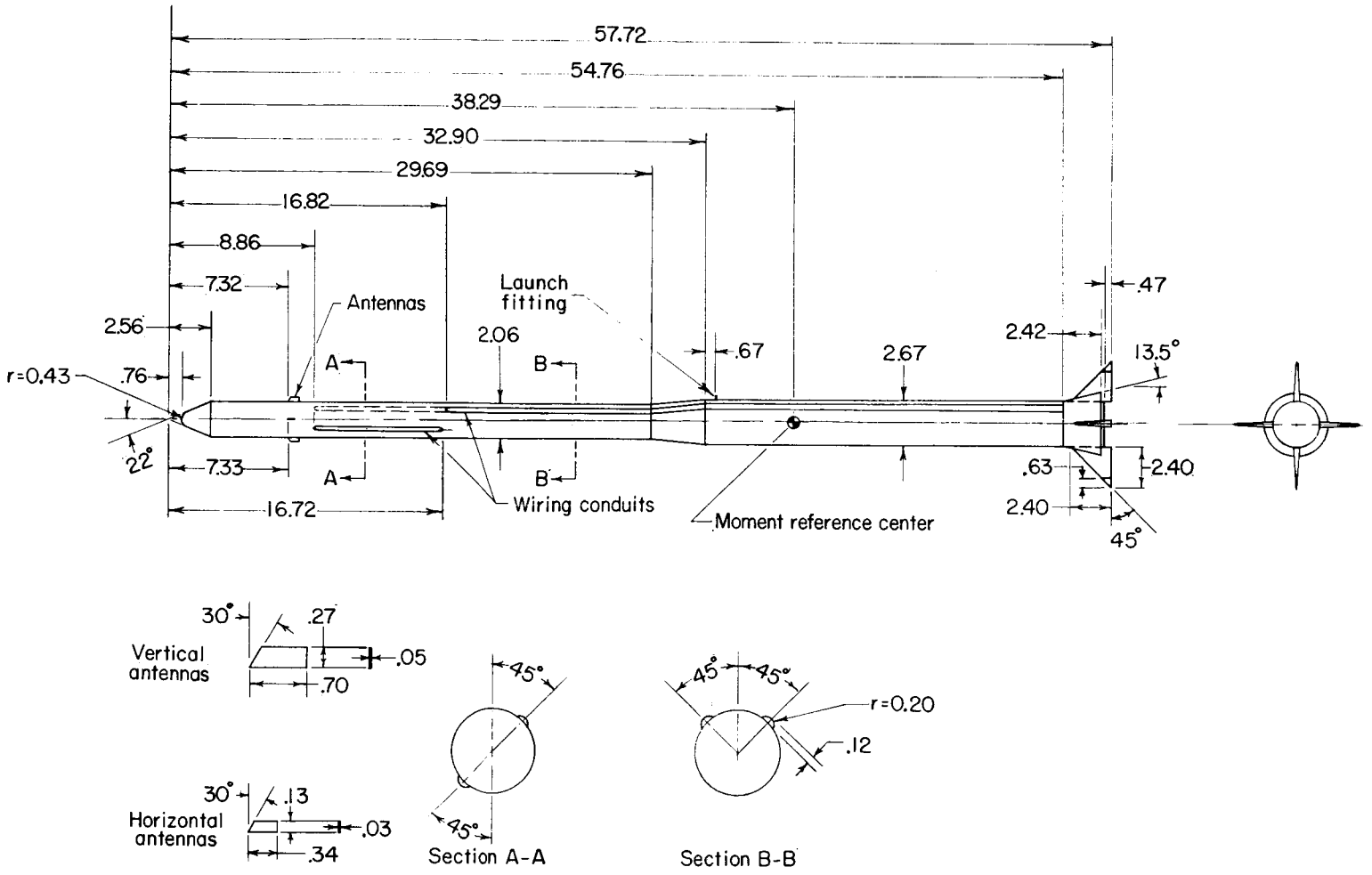

(a) Basic configuration. (Configuration G).

Figure 1.- Model details. All dimensions are in inches unless otherwise noted.

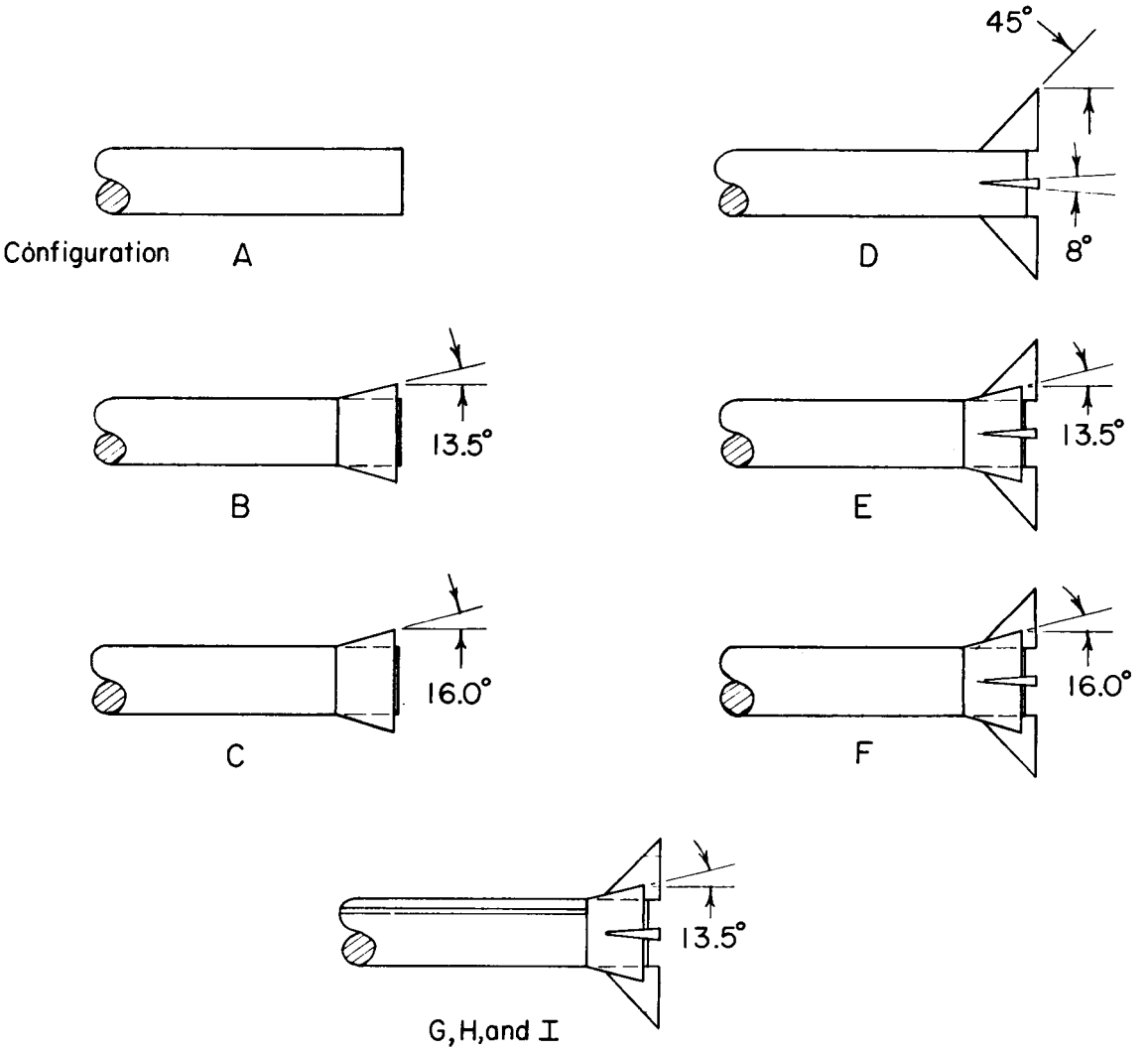

Configuration	Fins	Protuberances	δ_f, deg	δ_t, deg
A	Off	Off	0	0
B	Off	Off	13.5	0
C	Off	Off	16.0	0
D	On	Off	0	0
E	On	Off	13.5	0
F	On	Off	16.0	0
G	On	On	13.5	0
H	On	On	13.5	10
I	On	Antennas off only	13.5	0

(b) Model configurations.

Figure 1.- Concluded.

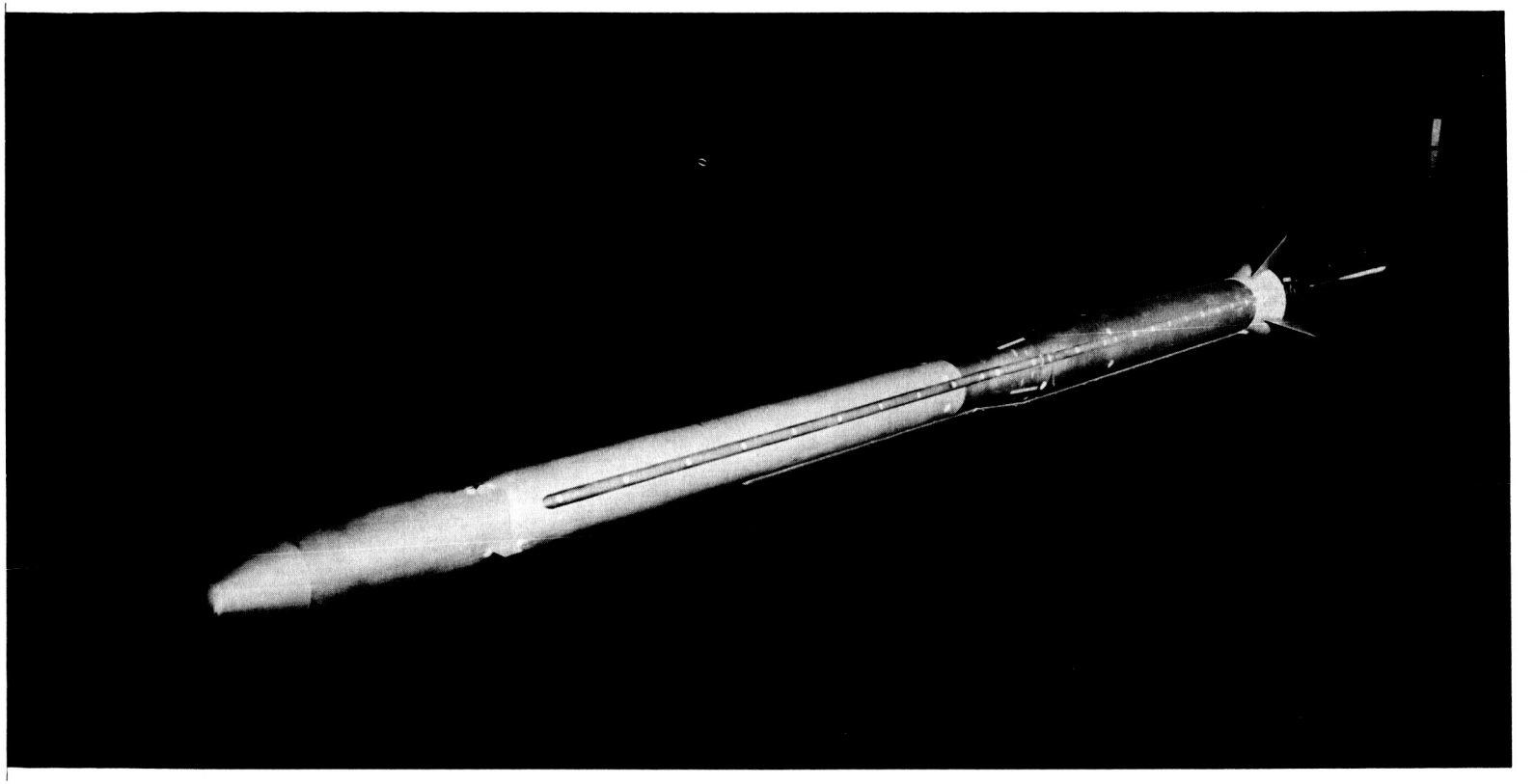

(a) Three-quarter front view.

L-60-2113

Figure 2.- Photographs of basic configuration.

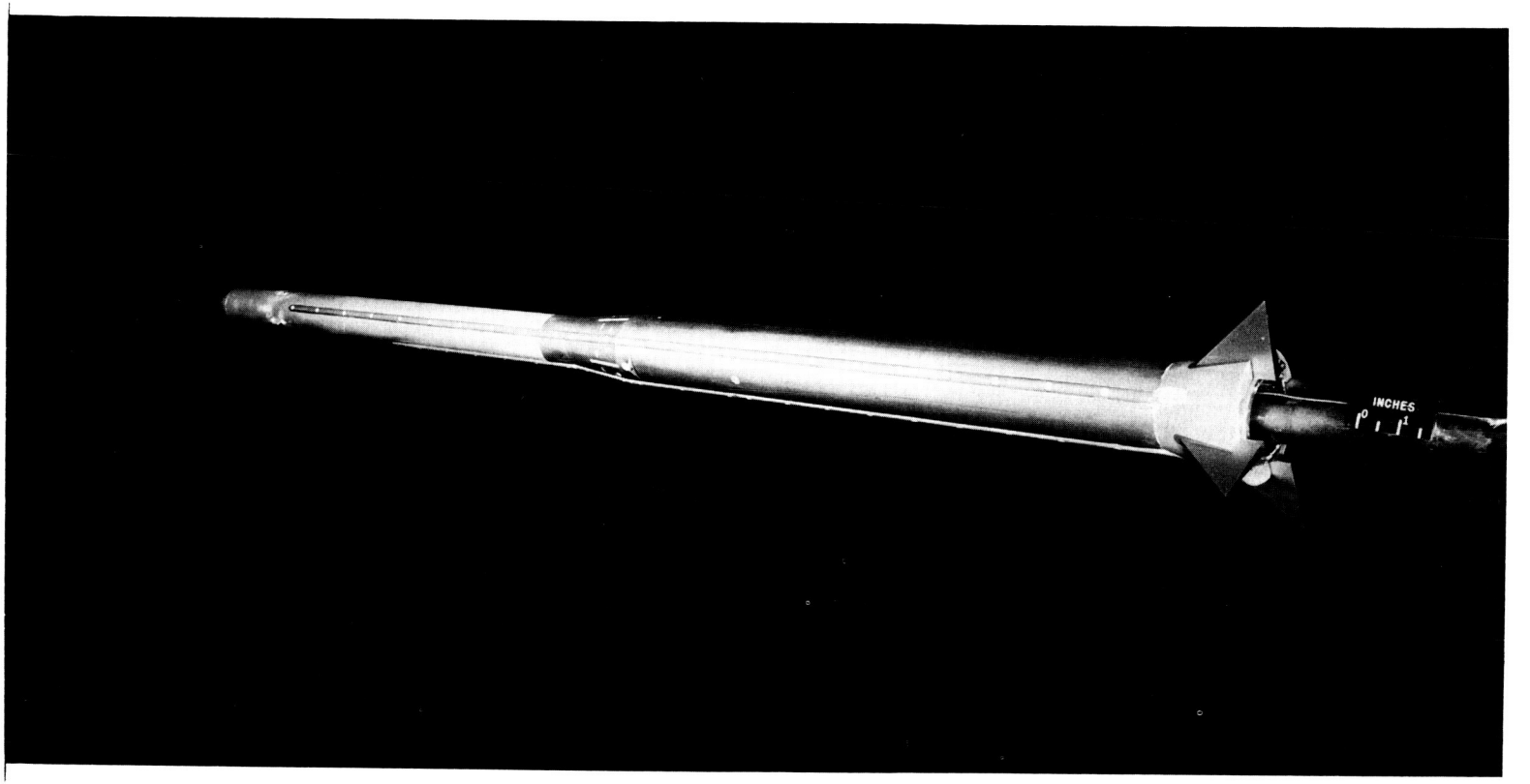

(b) Three-quarter rear view.

L-60-2111

Figure 2.- Concluded.

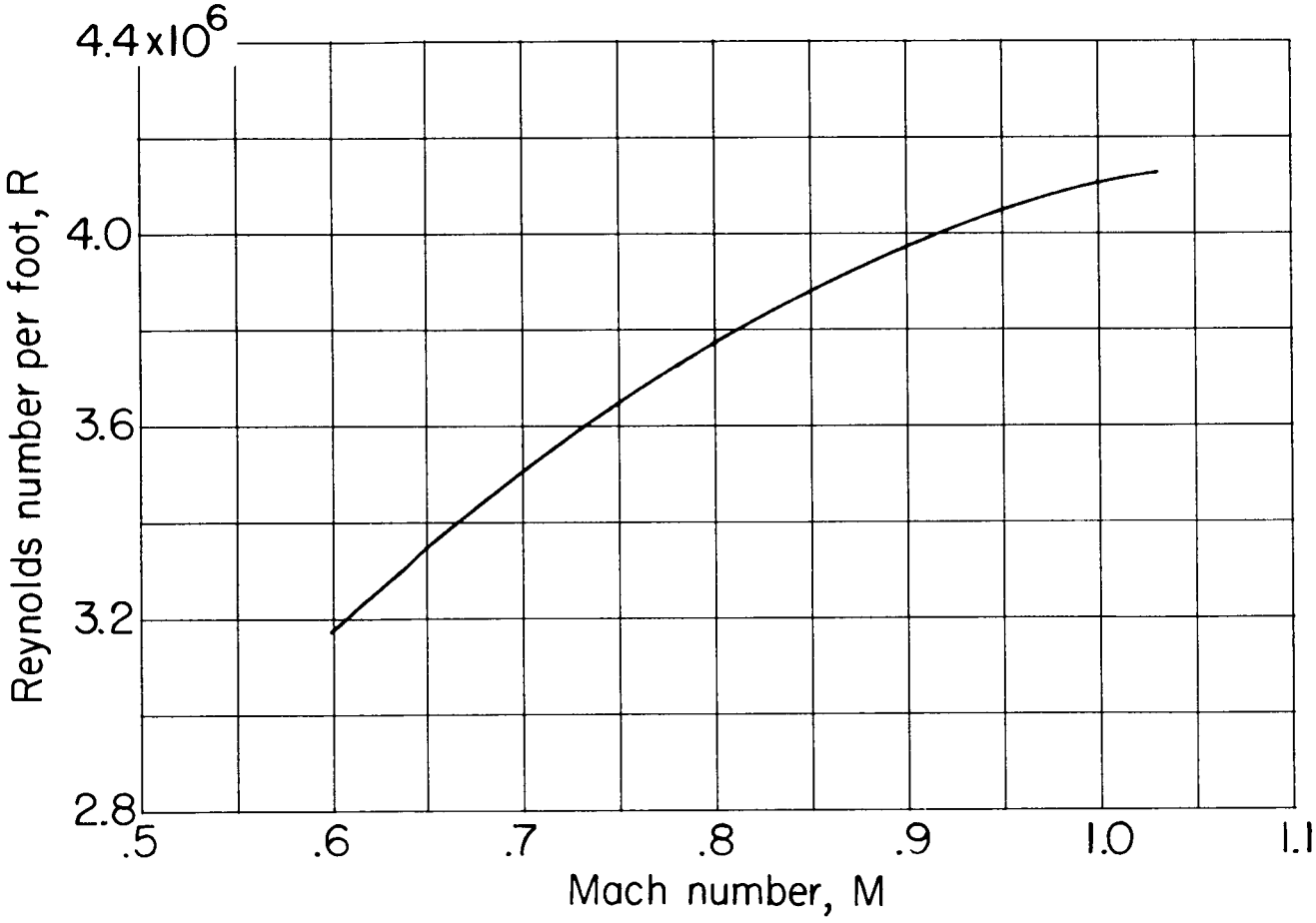

Figure 3.- Variation of average test Reynolds number per foot with Mach number.

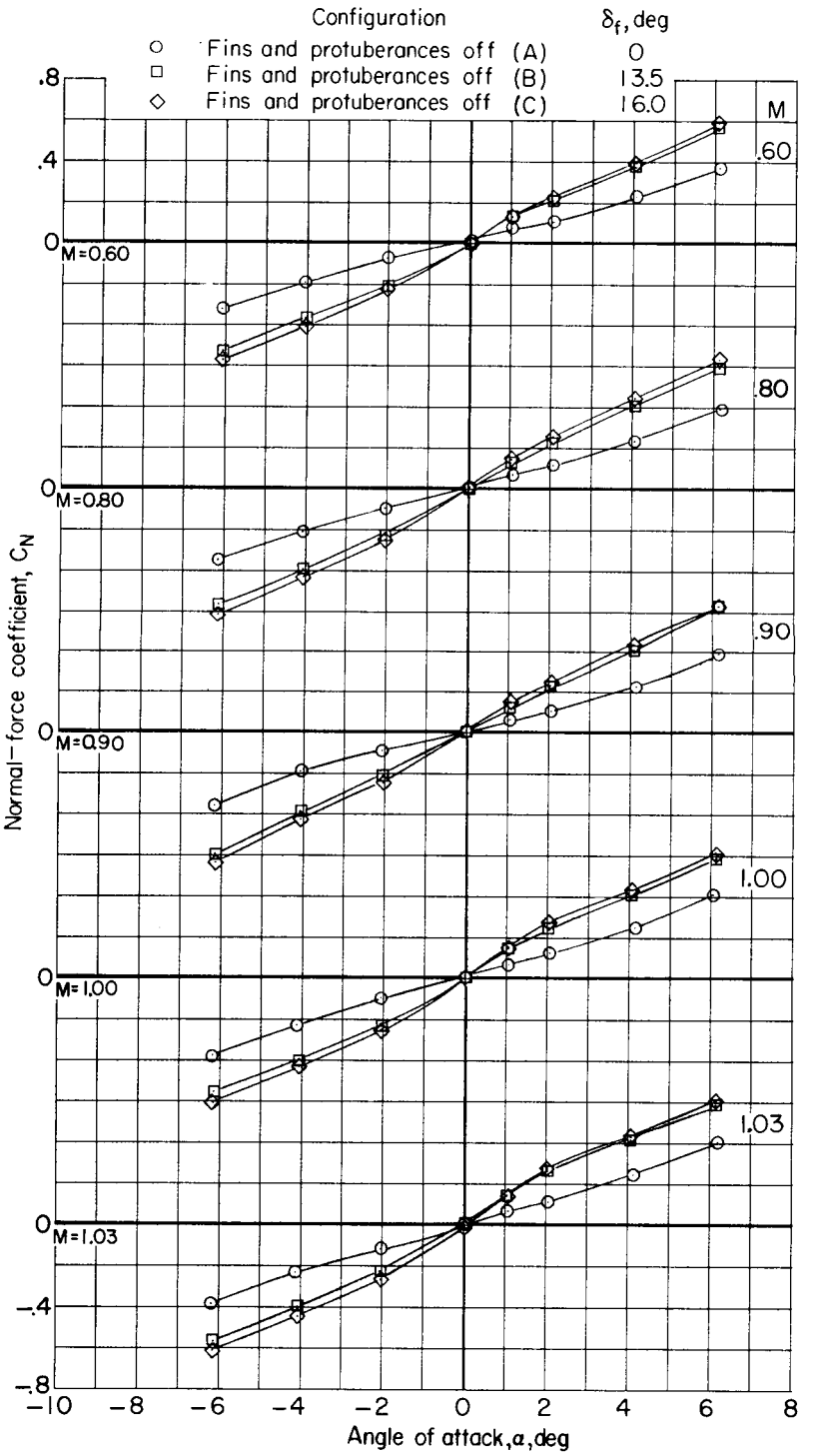

(a) Configurations A, B, and C.

Figure 4.- Variation with angle of attack of normal-force characteristics.

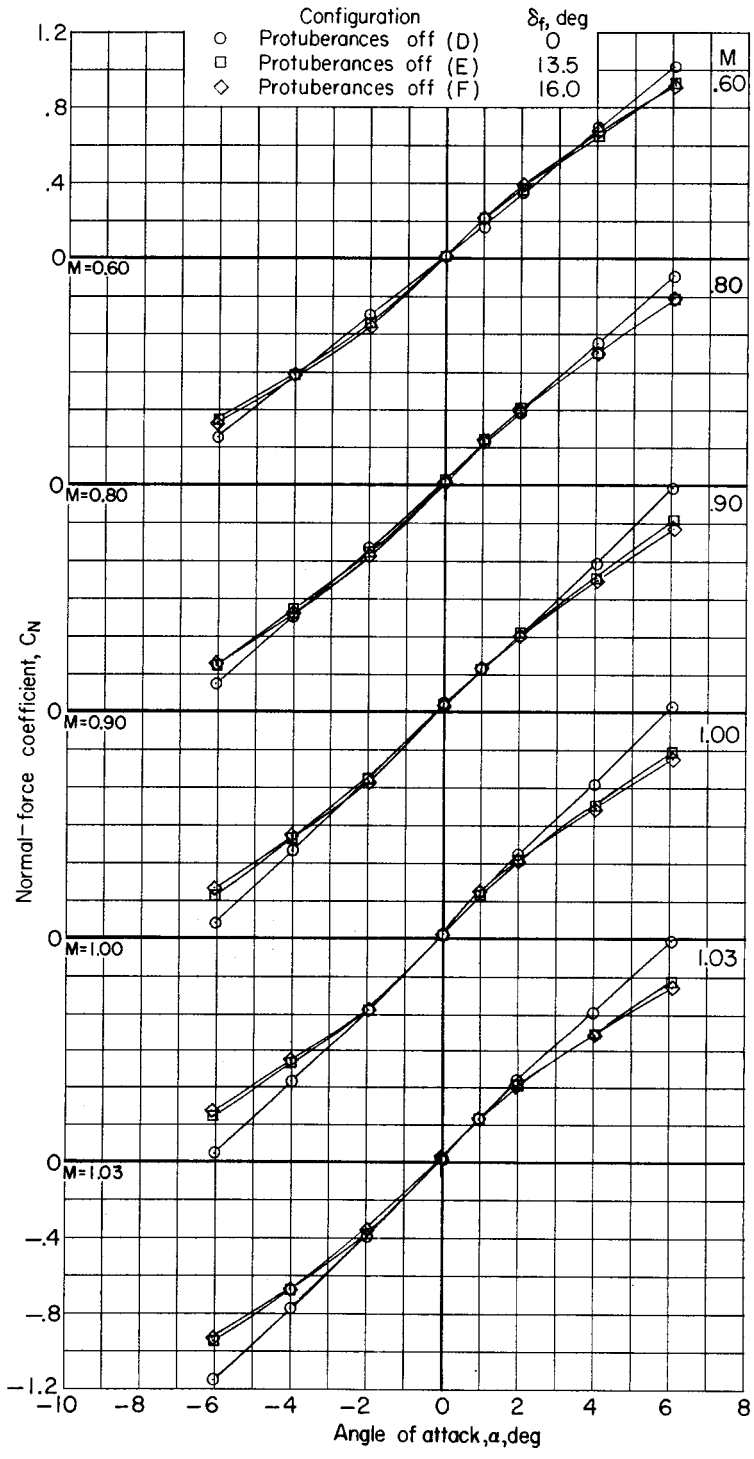

(b) Configurations D, E, and F.

Figure 4.- Continued.

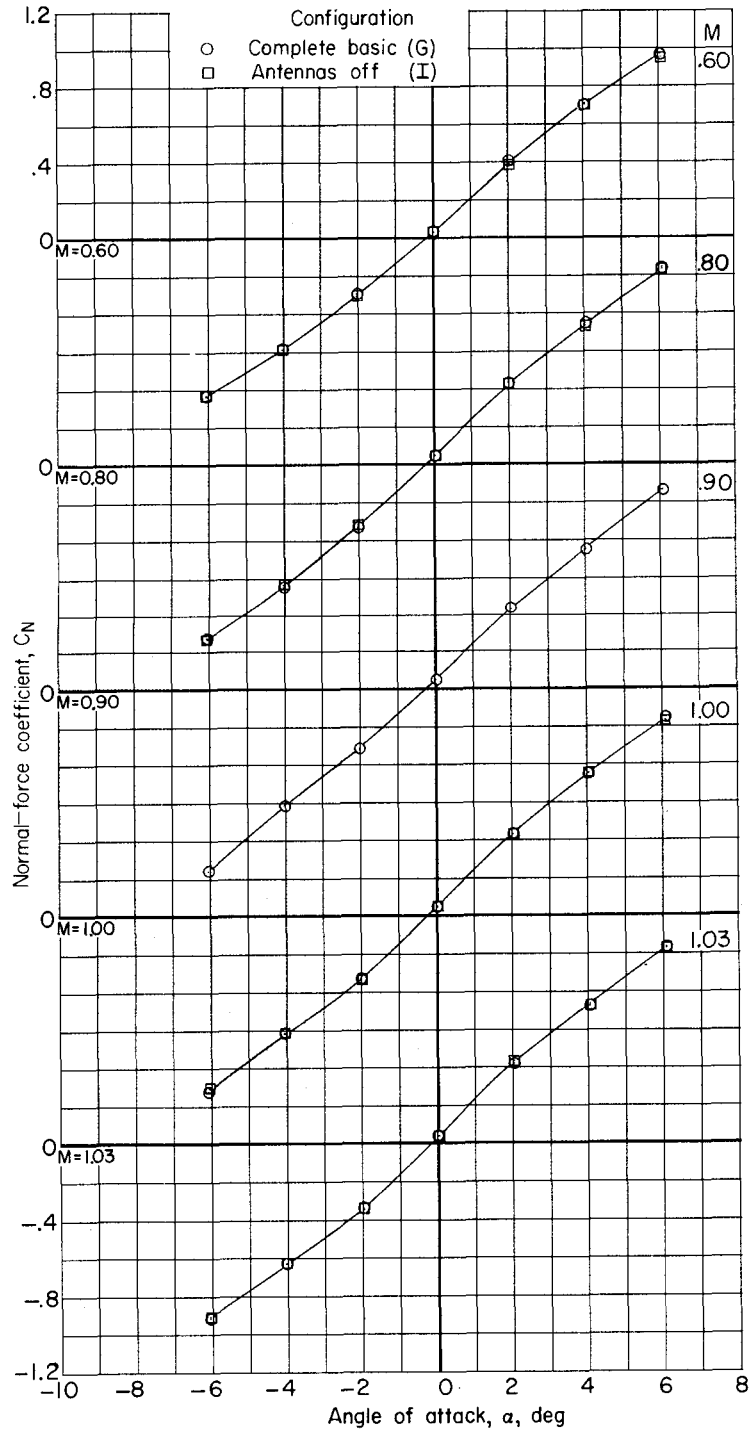

(c) Configurations G and I.

Figure 4.- Concluded.

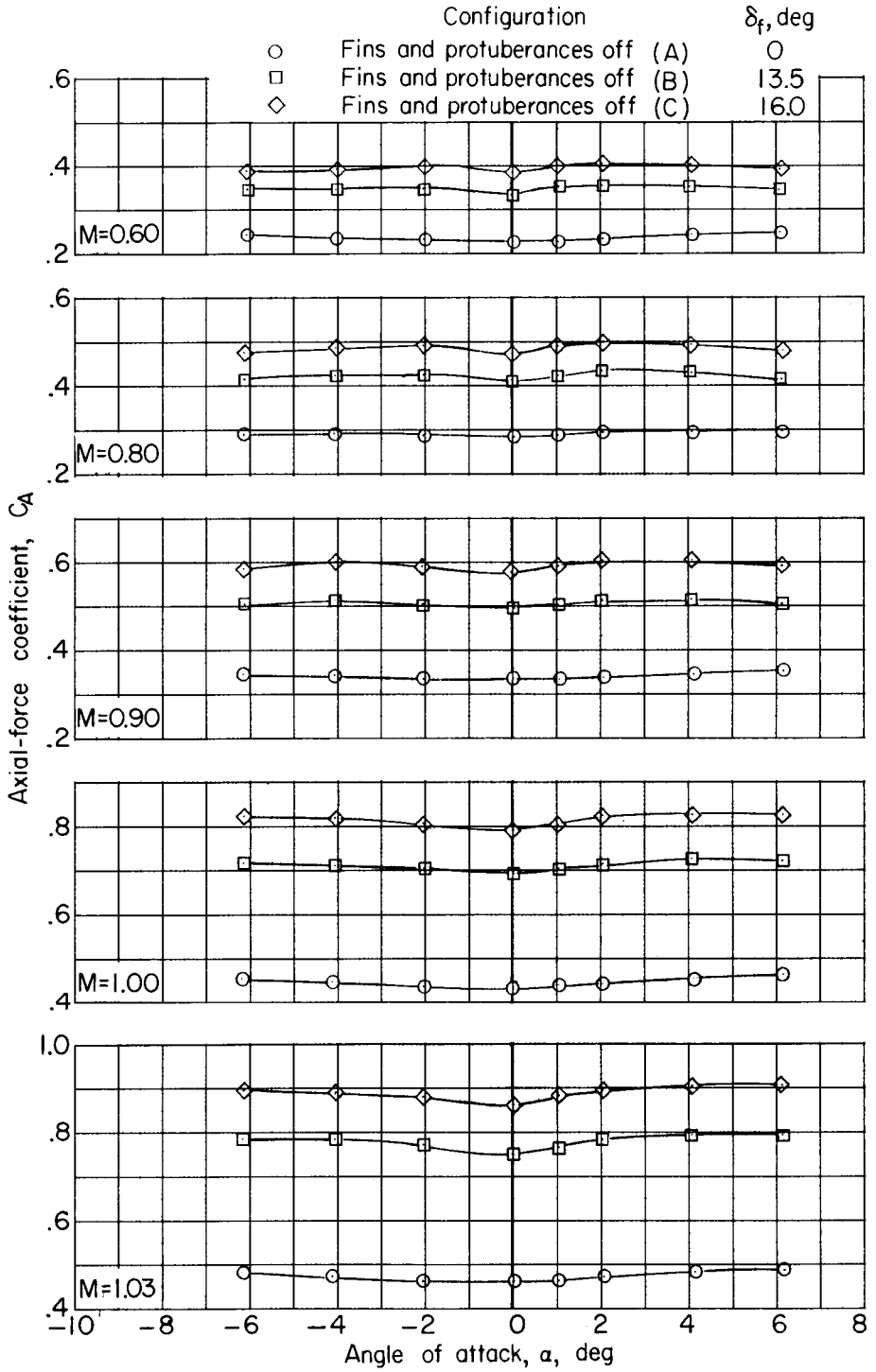

(a) Axial-force coefficients; configurations A, B, and C.

Figure 5.- Variation with angle of attack of axial-force characteristics.

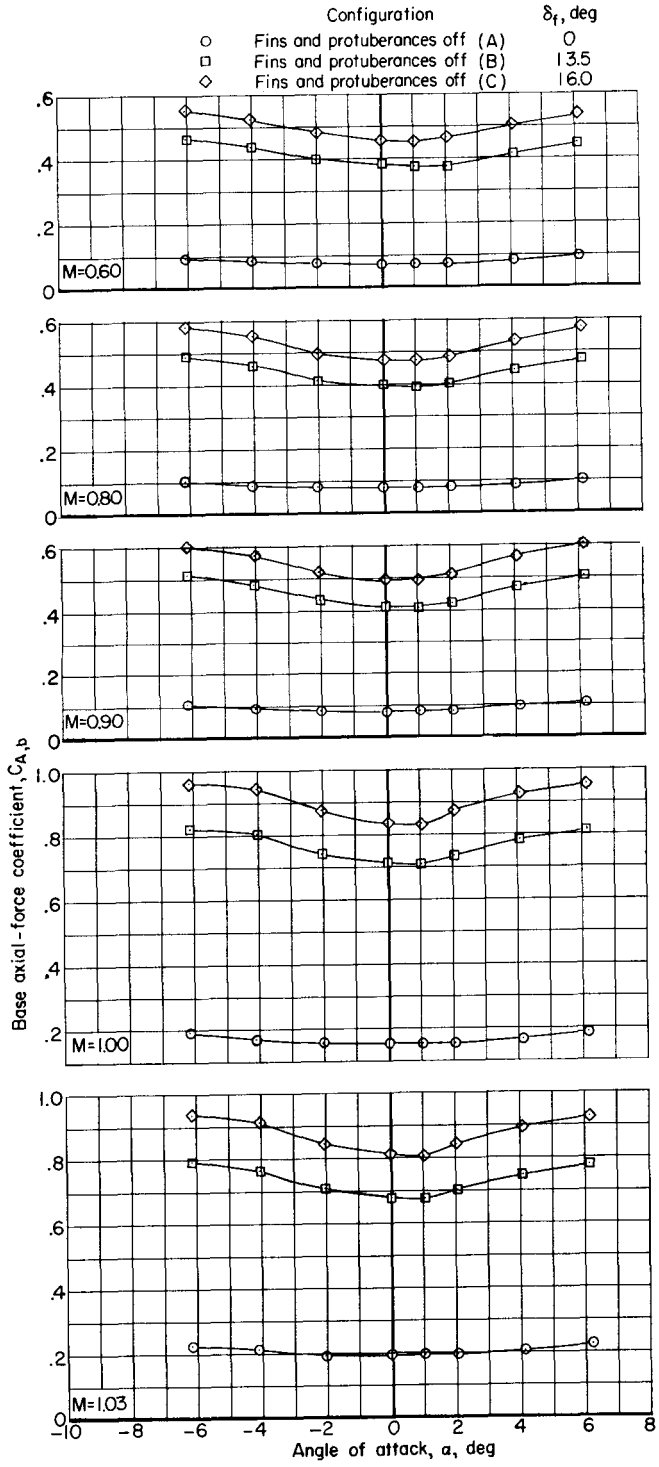

(b) Base axial-force coefficients; configurations A, B, and C.

Figure 5.- Continued.

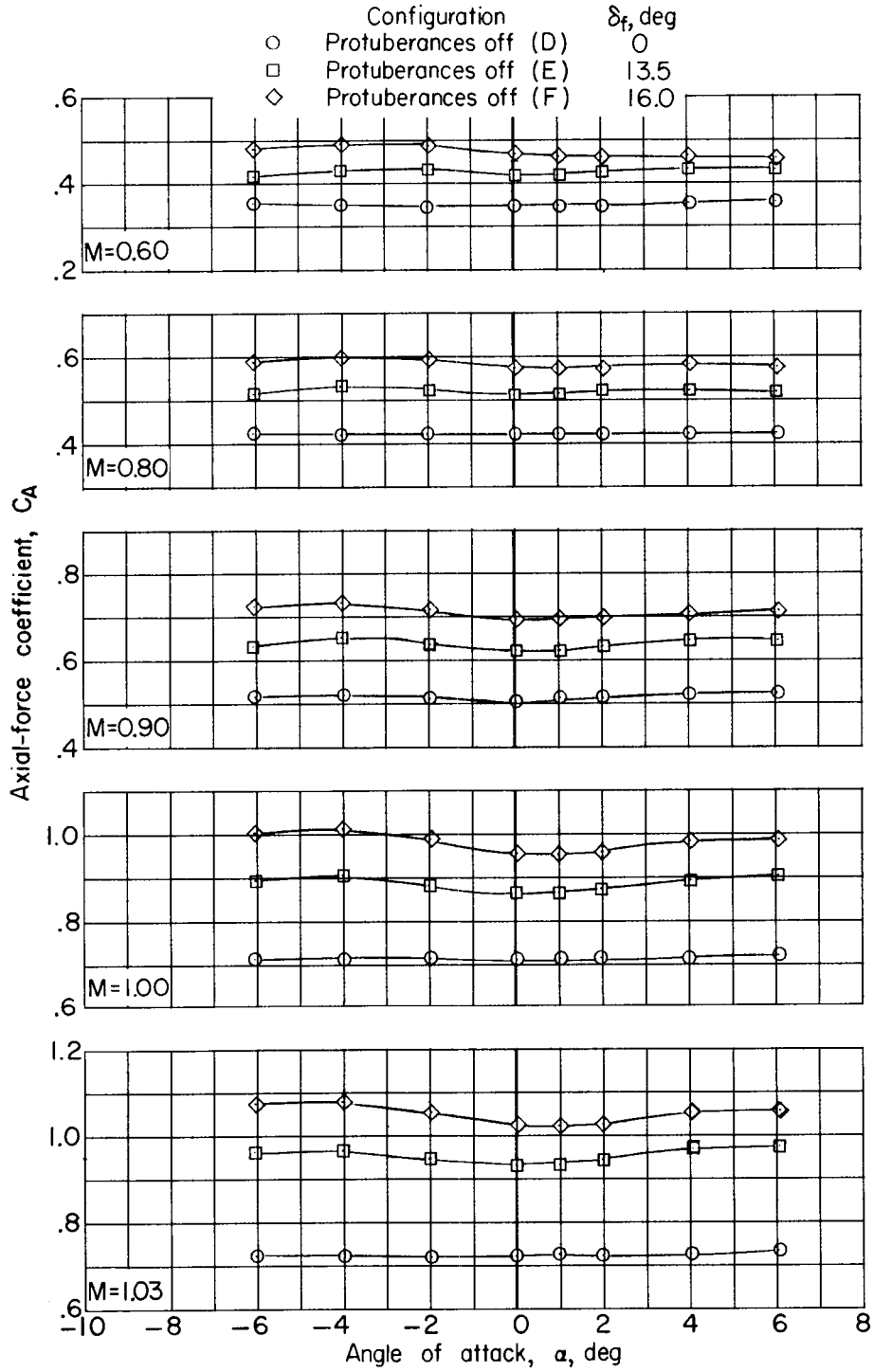

(c) Axial-force coefficients; configurations D, E, and F.

Figure 5.- Continued.

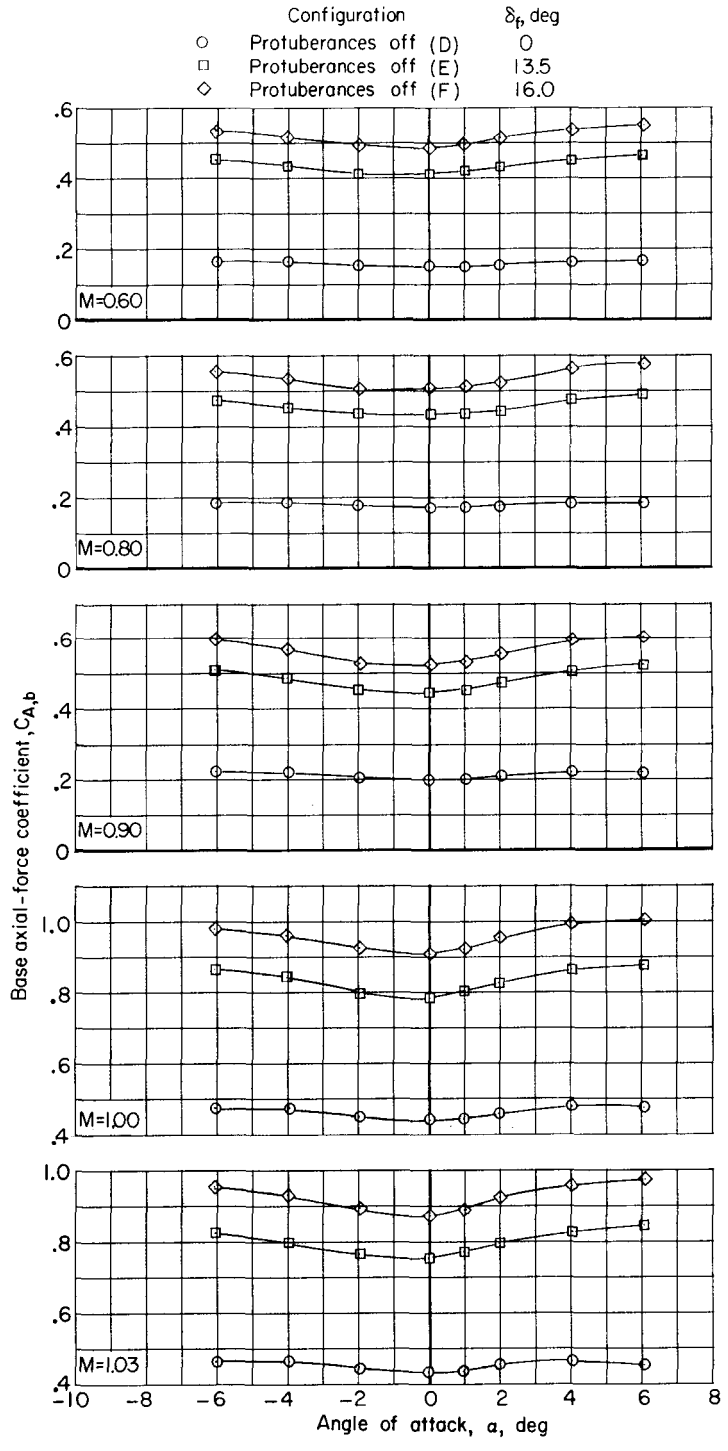

(d) Base axial-force coefficients; configurations D, E, and F.

Figure 5.- Continued.

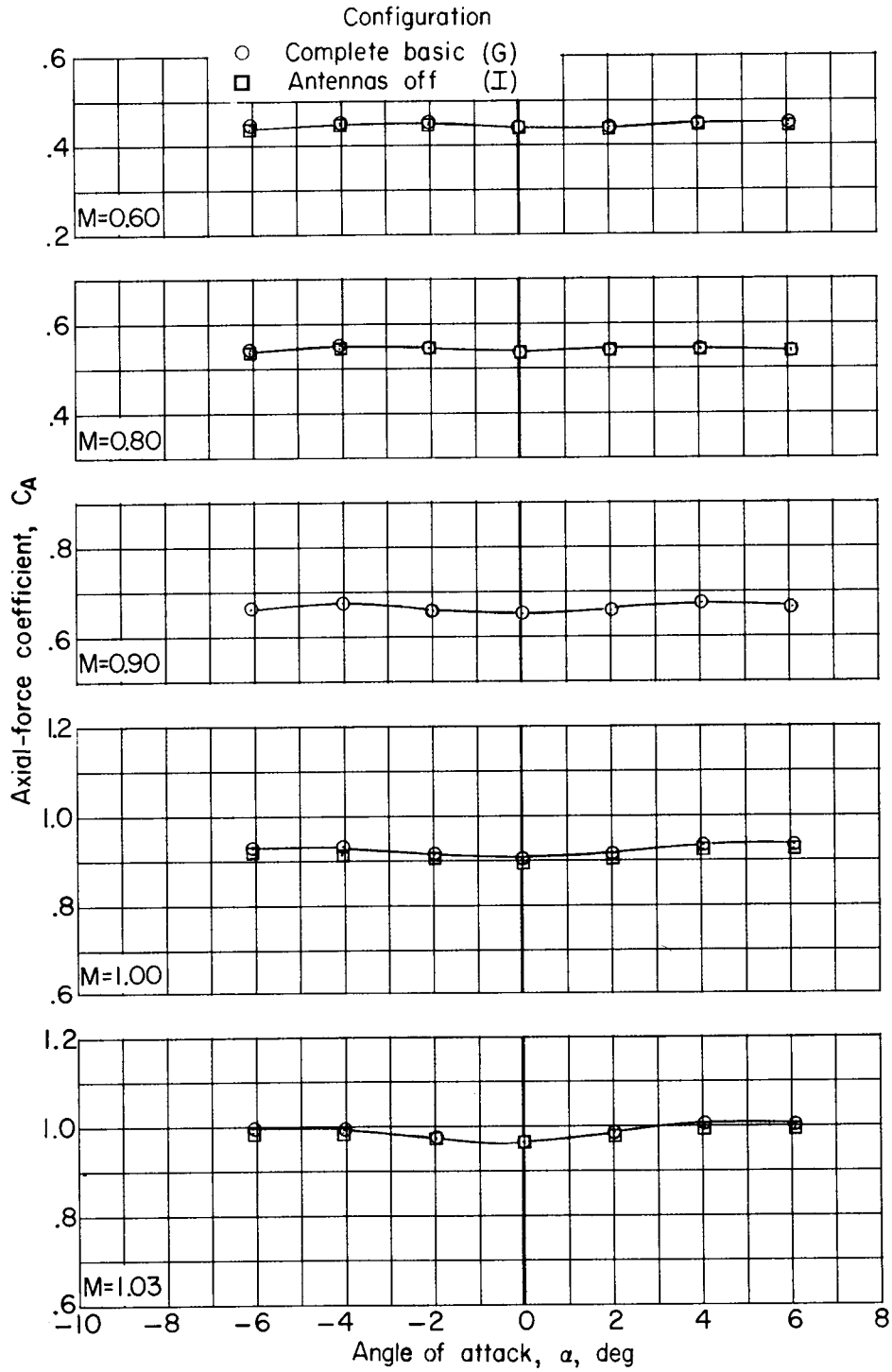

(e) Axial-force coefficients; configurations G and I.

Figure 5.- Continued.

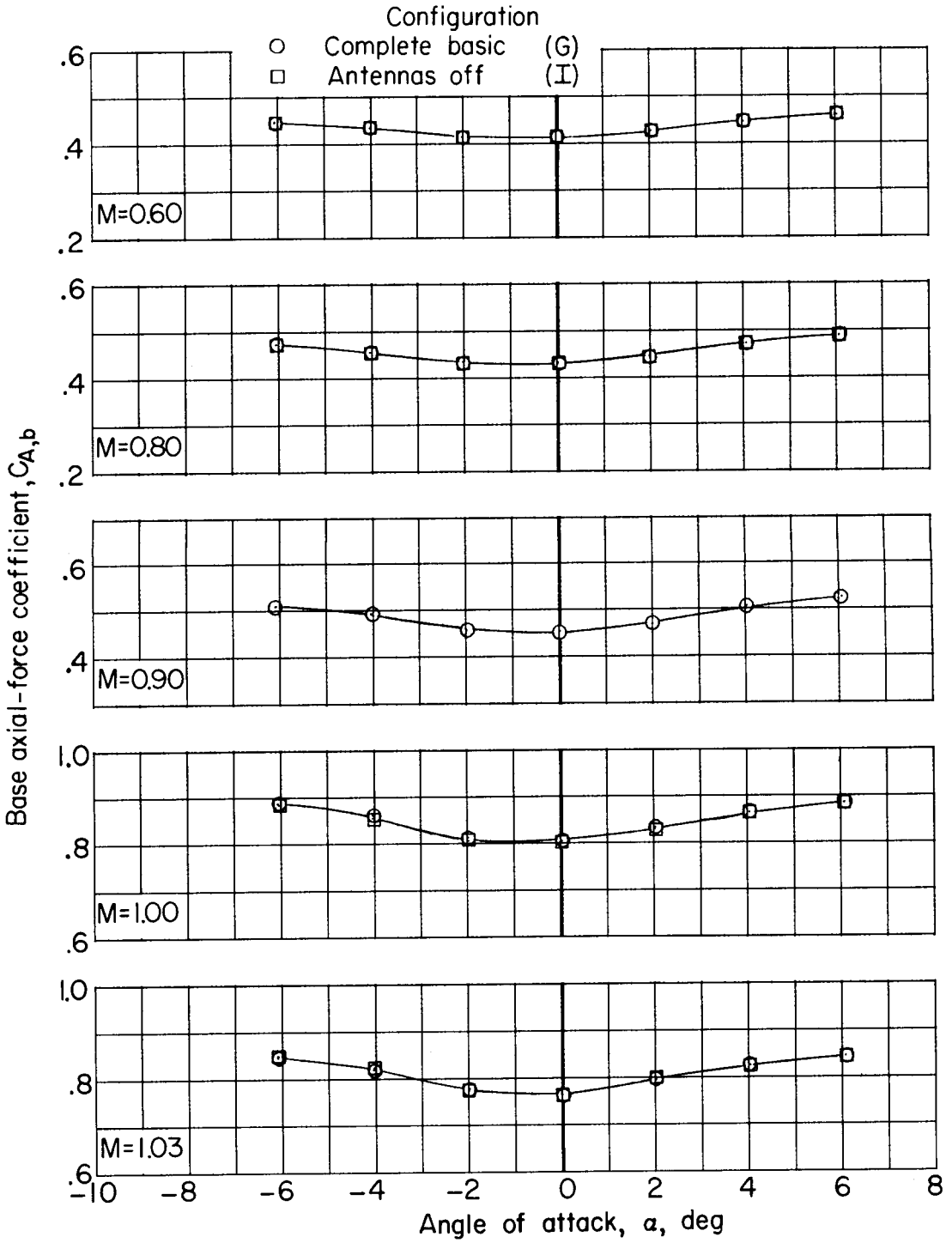

(f) Base axial-force coefficients; configurations G and I.

Figure 5.- Concluded.

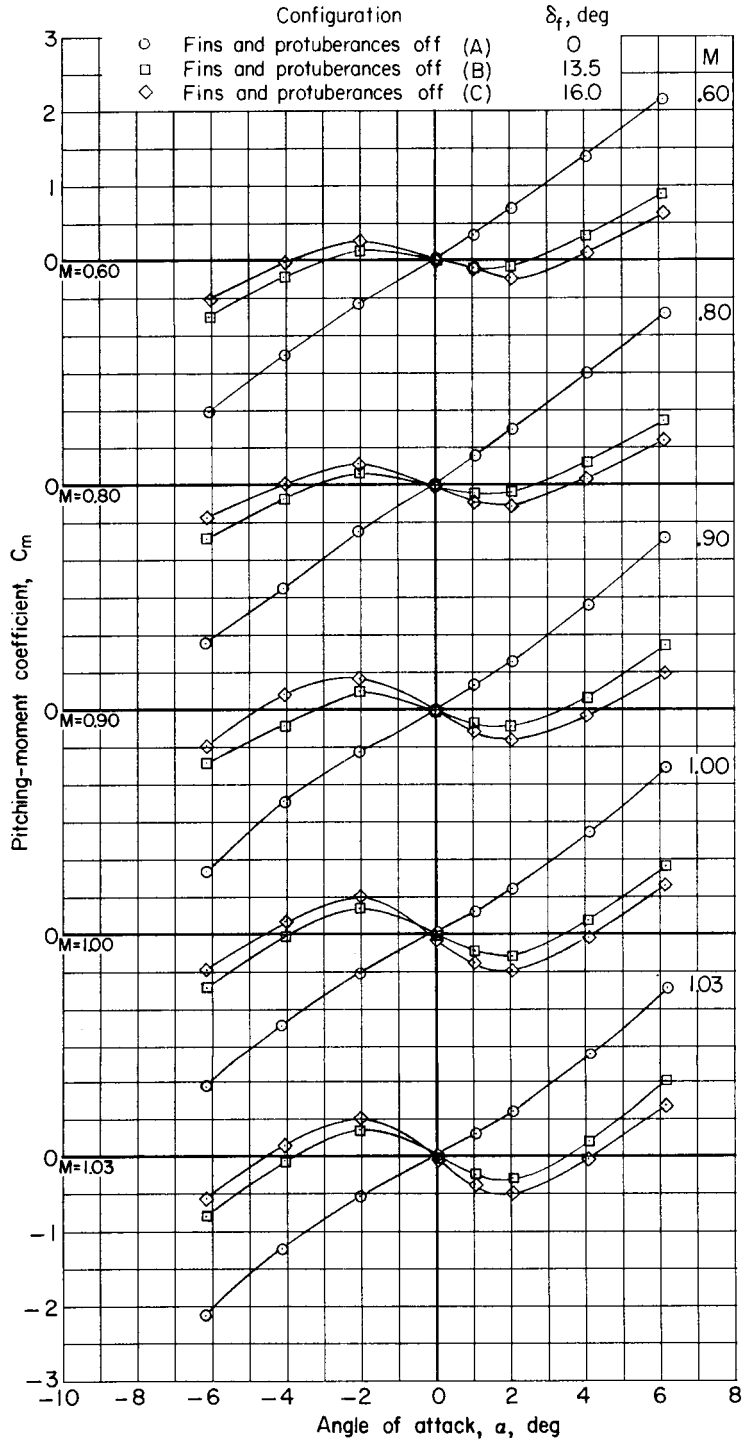

(a) Configurations A, B, and C.

Figure 6.- Variation with angle of attack of pitching-moment characteristics.

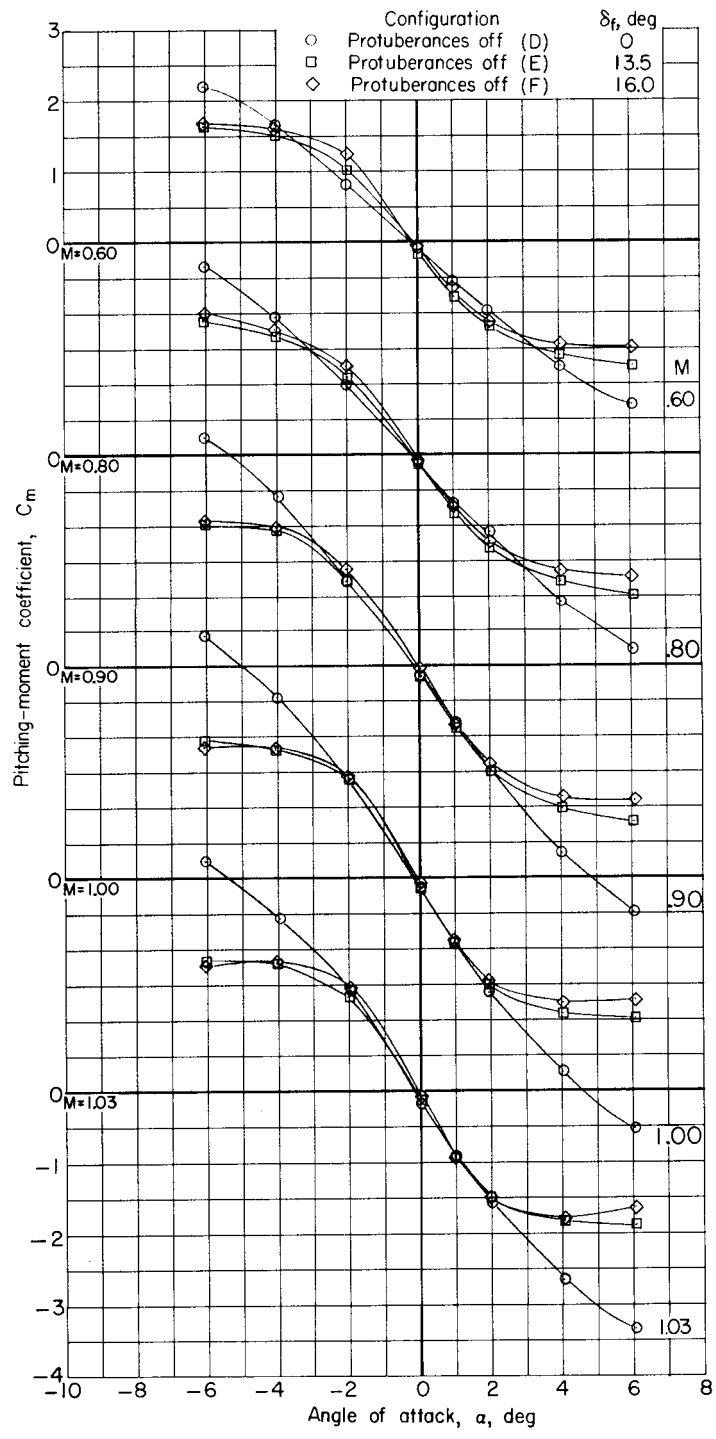

(b) Configurations D, E, and F.

Figure 6.- Continued.

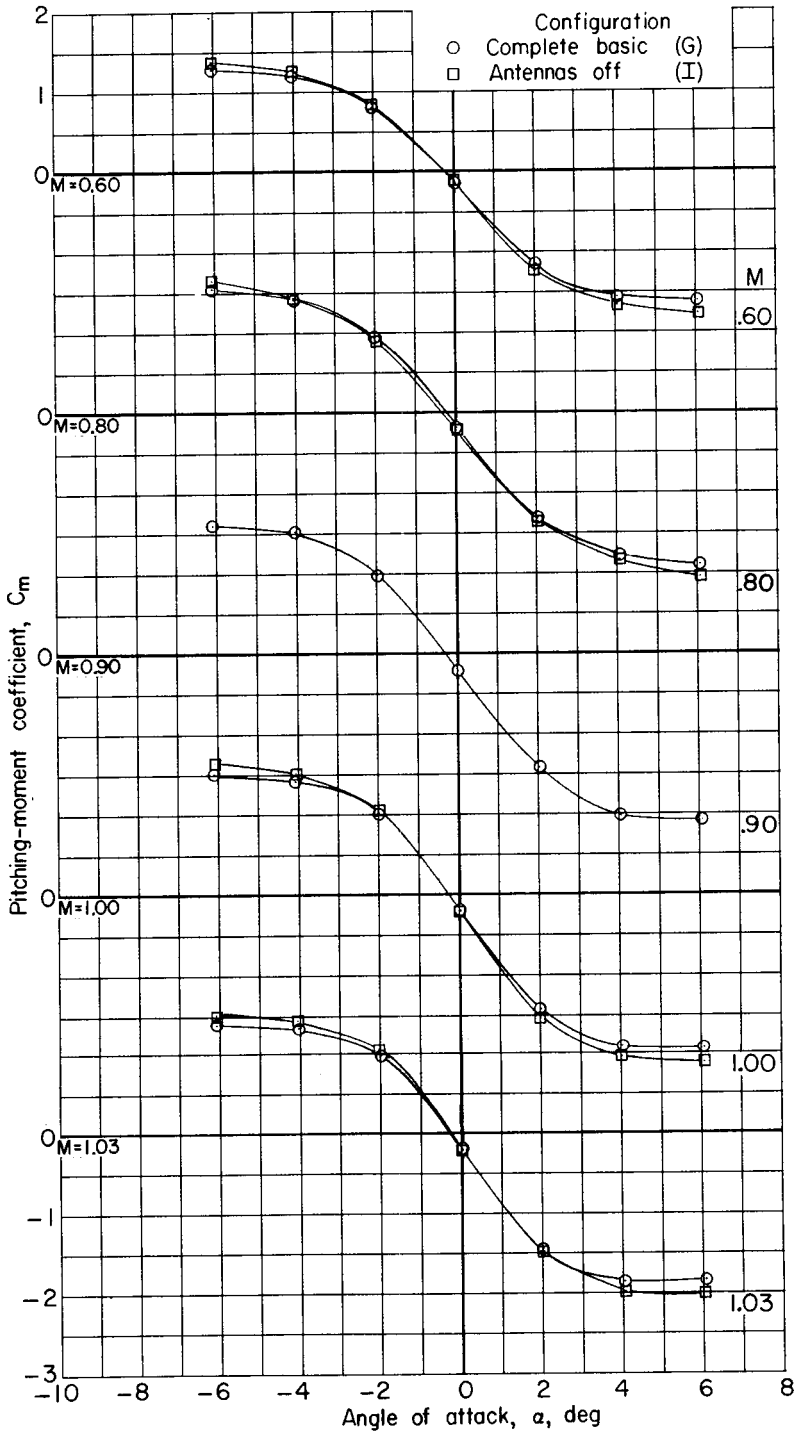

(c) Configurations G and I.

Figure 6.- Concluded.

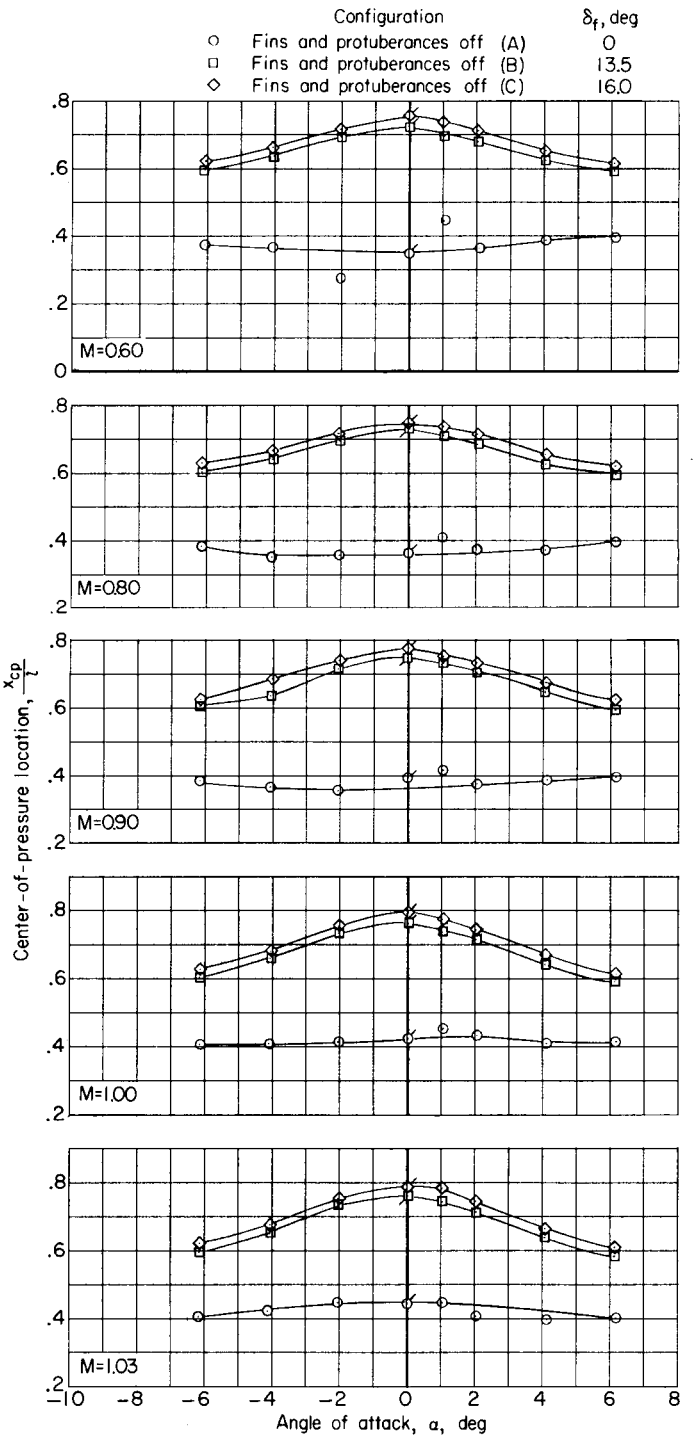

(a) Configurations A, B, and C.

Figure 7.- Variation with angle of attack of longitudinal center-of-pressure characteristics.

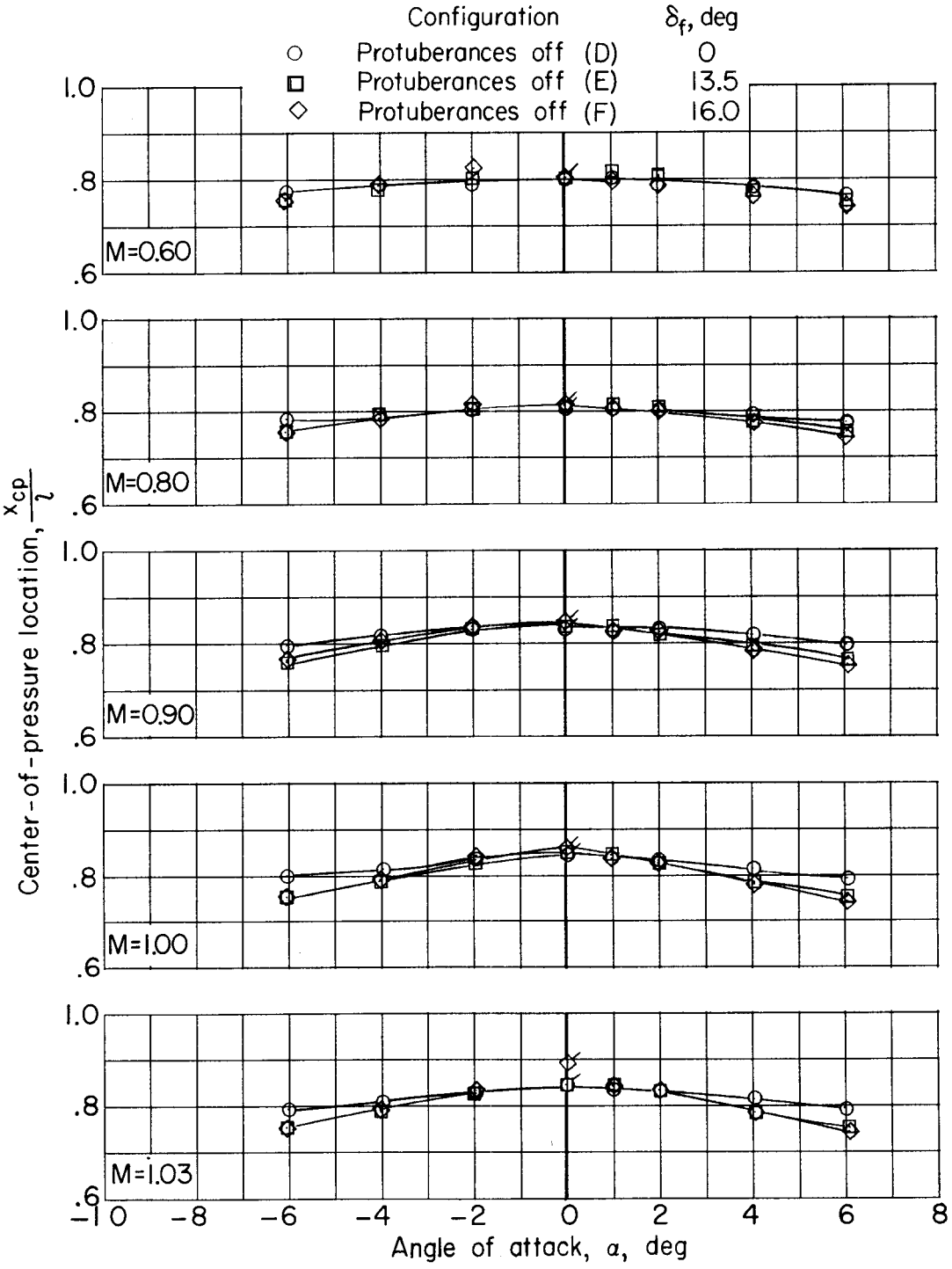

(b) Configurations D, E, and F.

Figure 7.- Continued.

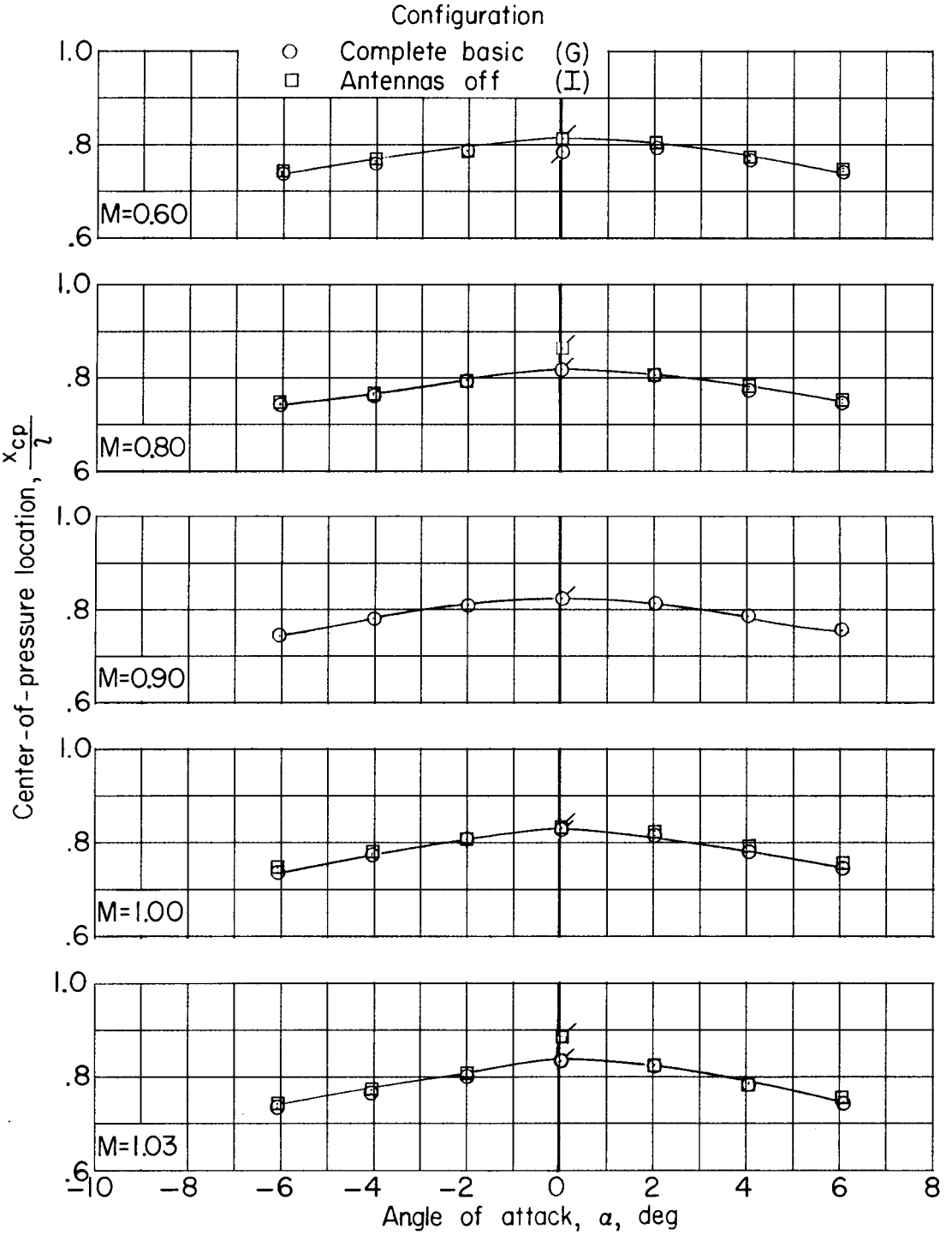

(c) Configurations G and I.

Figure 7.- Concluded.

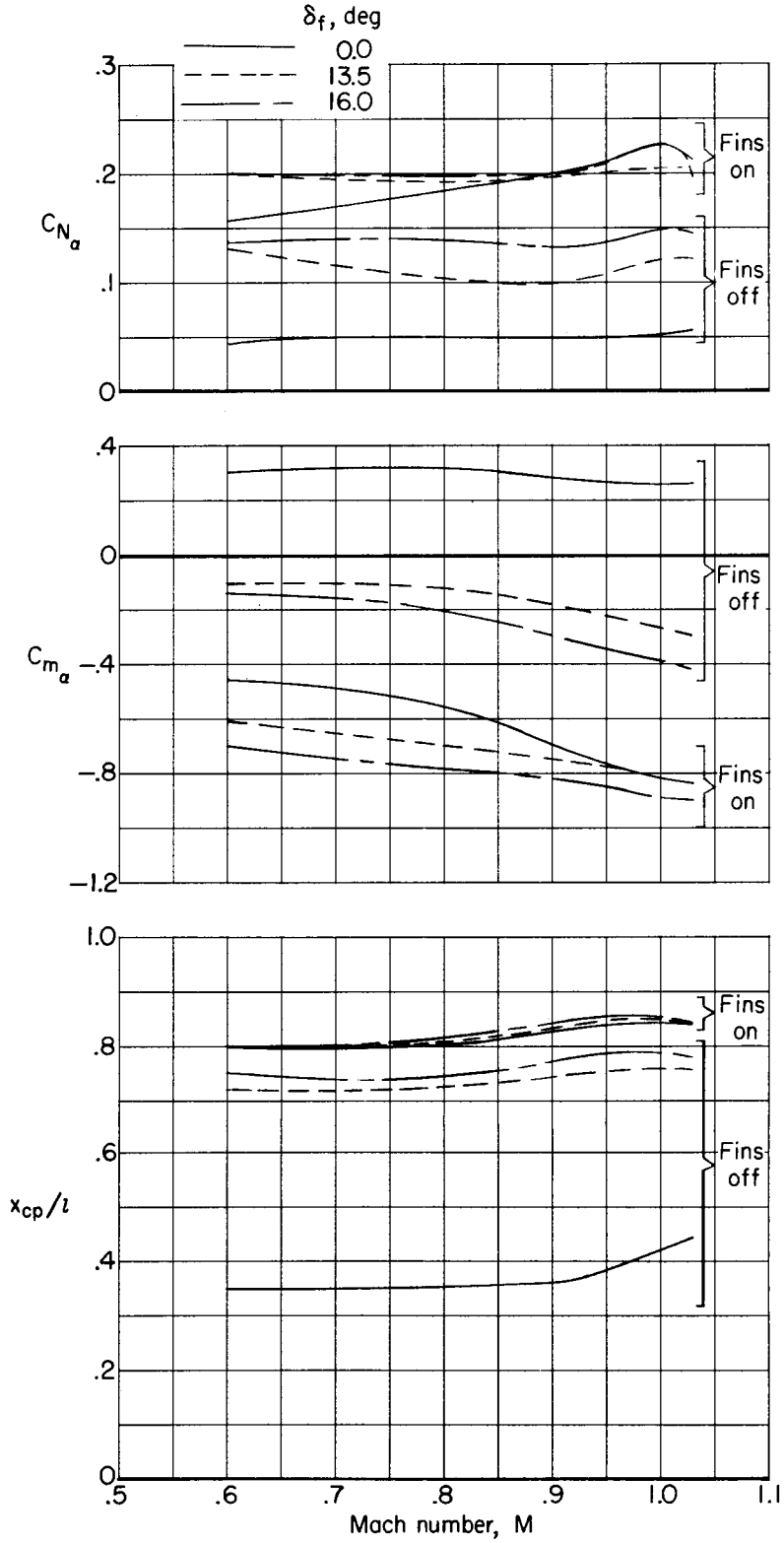

(a) C_{N_α}, C_{m_α}, and x_{cp}/l; effects of fins and flares.

Figure 8.- Summary of aerodynamic characteristics in pitch. $\alpha = 0^o$.

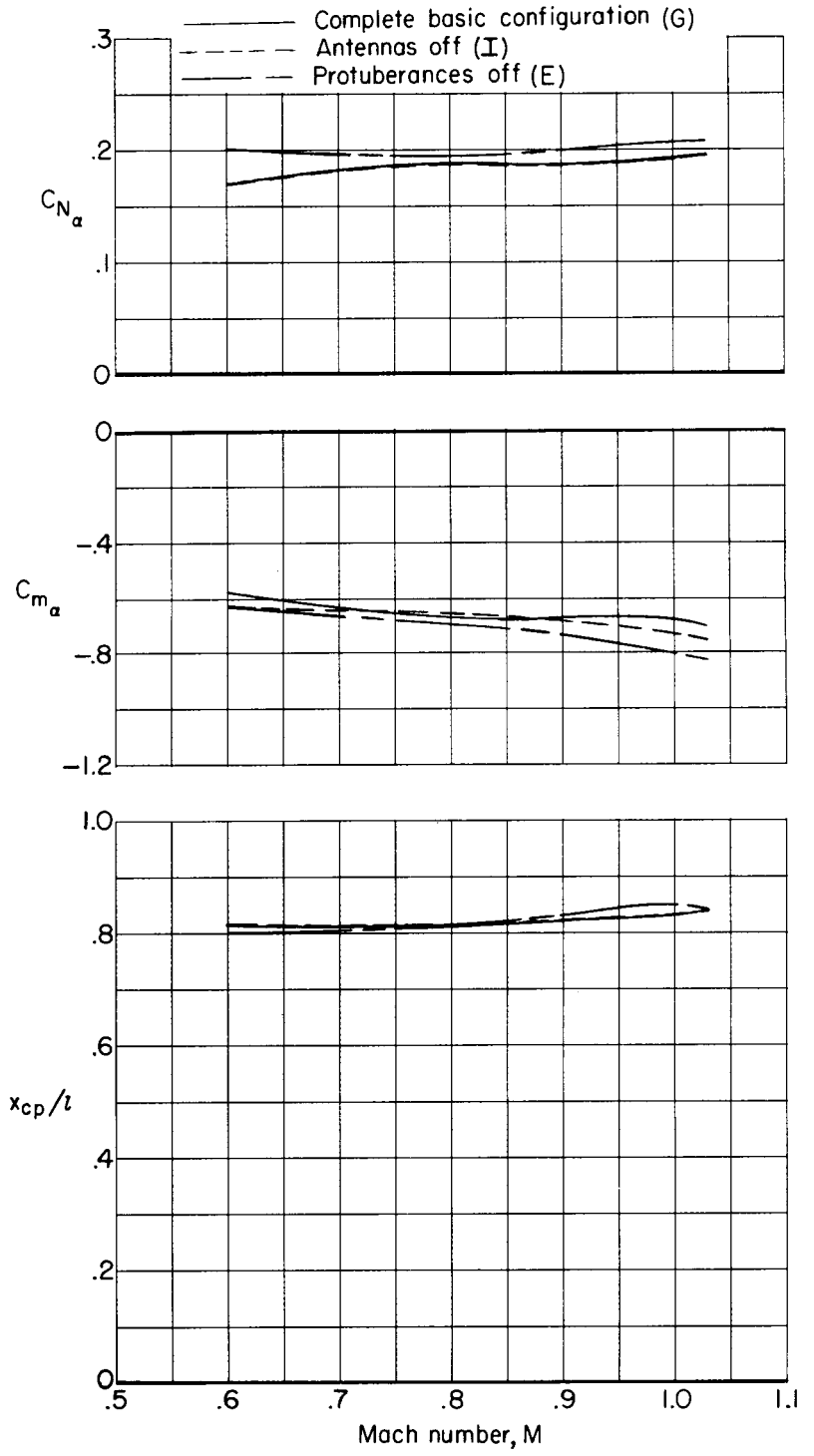

(b) C_{N_α}, C_{m_α}, and x_{cp}/l; effects of protuberances.

Figure 8.- Continued.

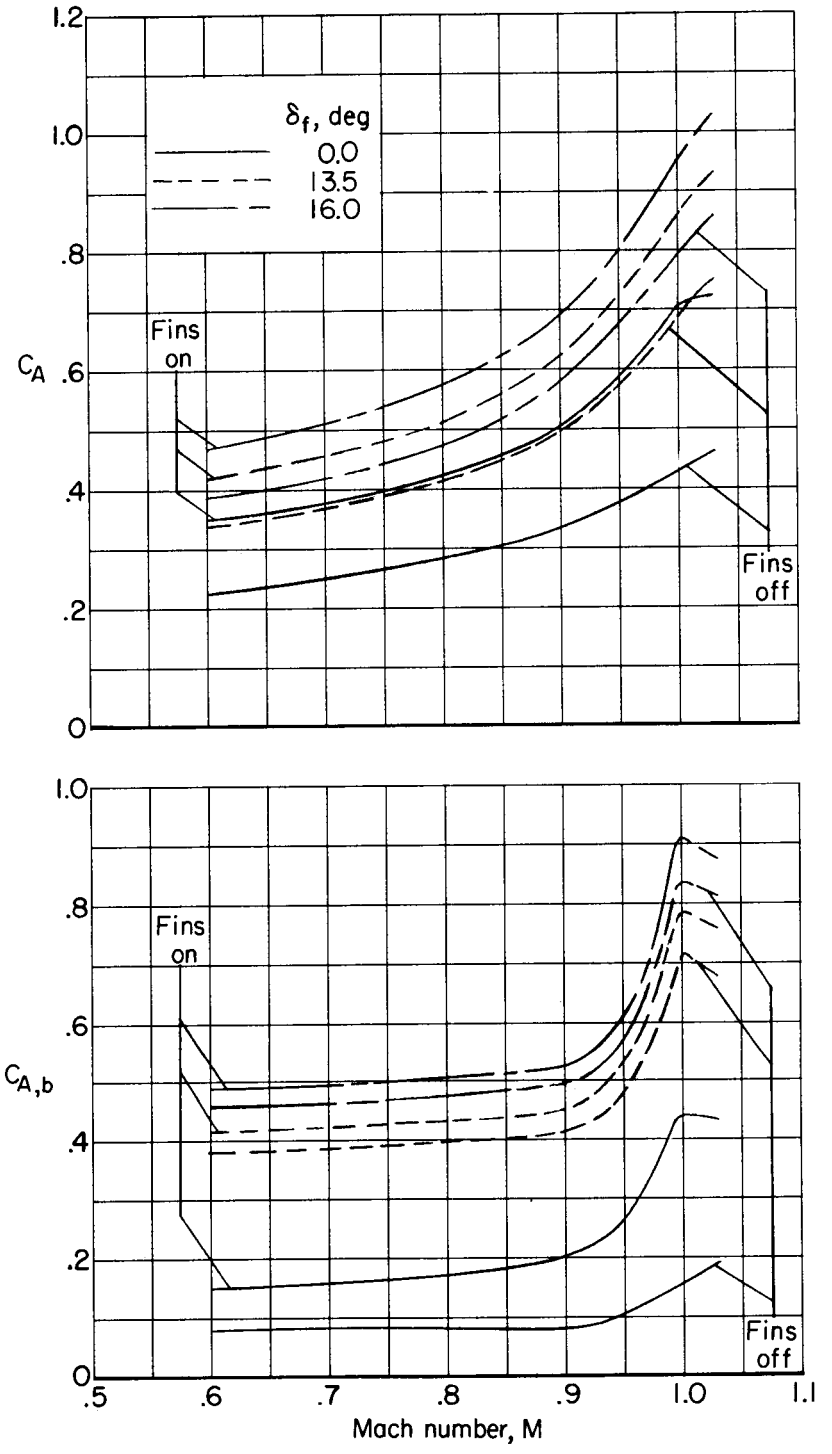

(c) C_A and $C_{A,b}$; effects of fins and flares.

Figure 8.- Continued.

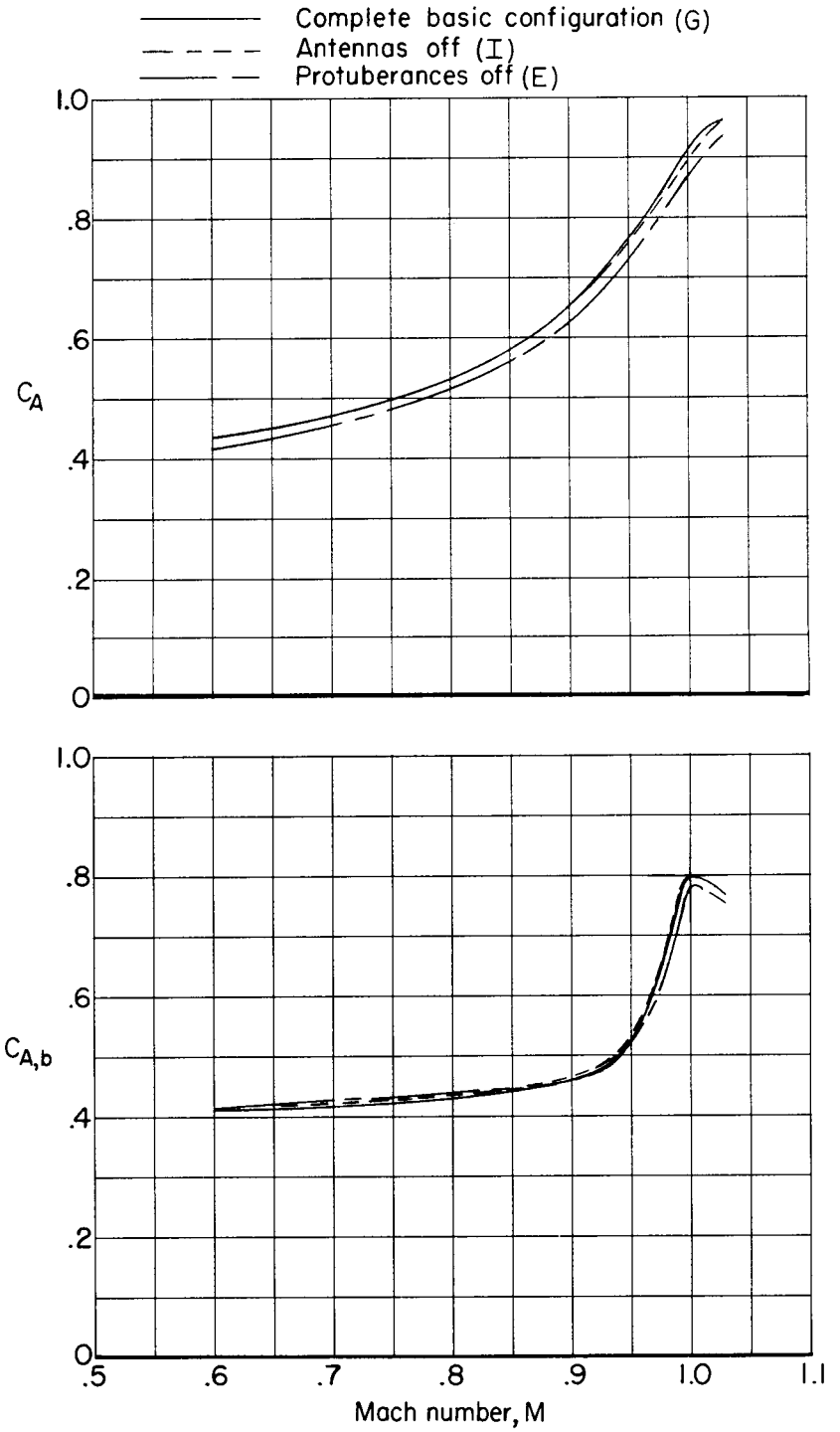

(d) C_A and $C_{A,b}$; effects of protuberances.

Figure 8.- Concluded.

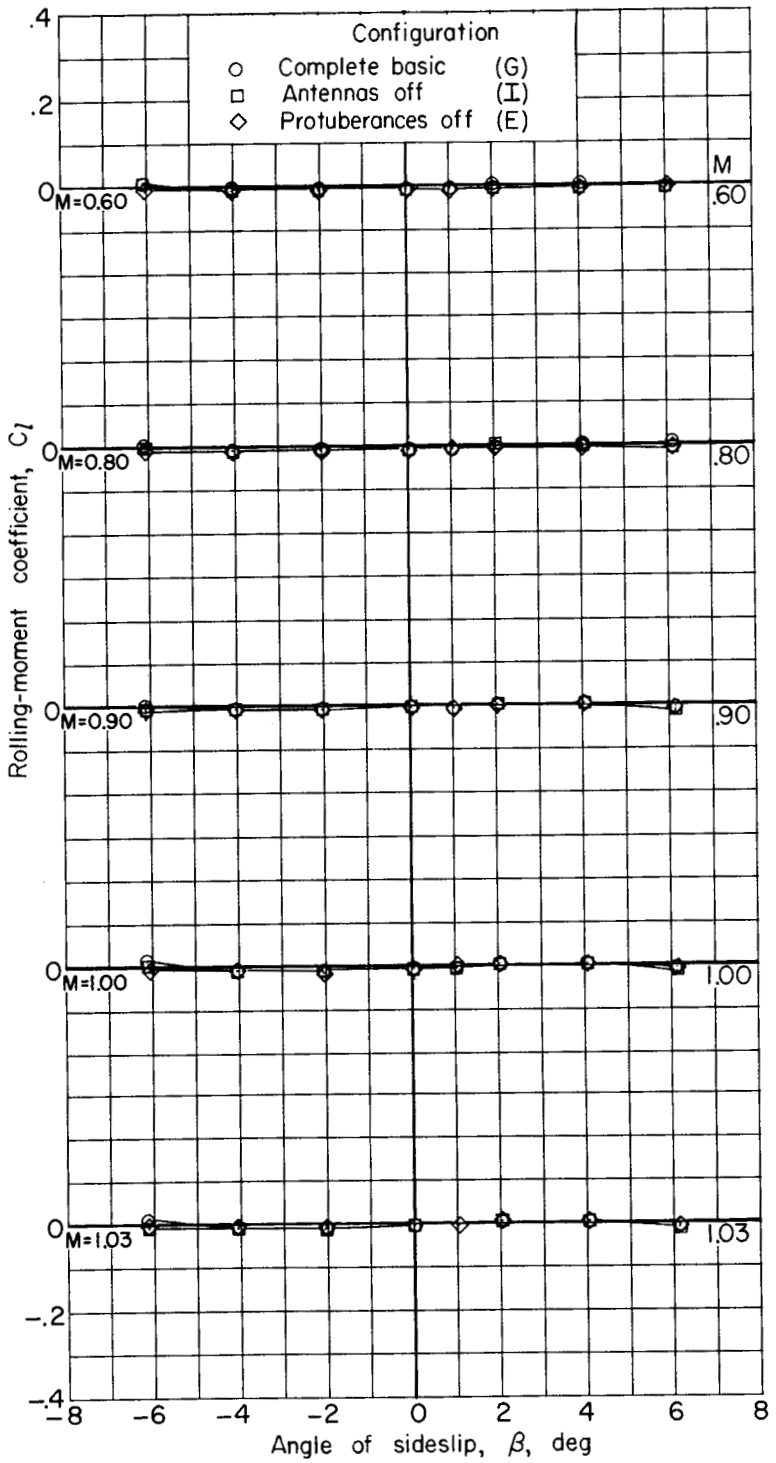

(a) $\alpha = 0^{\circ}$; configurations E, G, and I.

Figure 9.- Variation with angle of sideslip of rolling-moment characteristics.

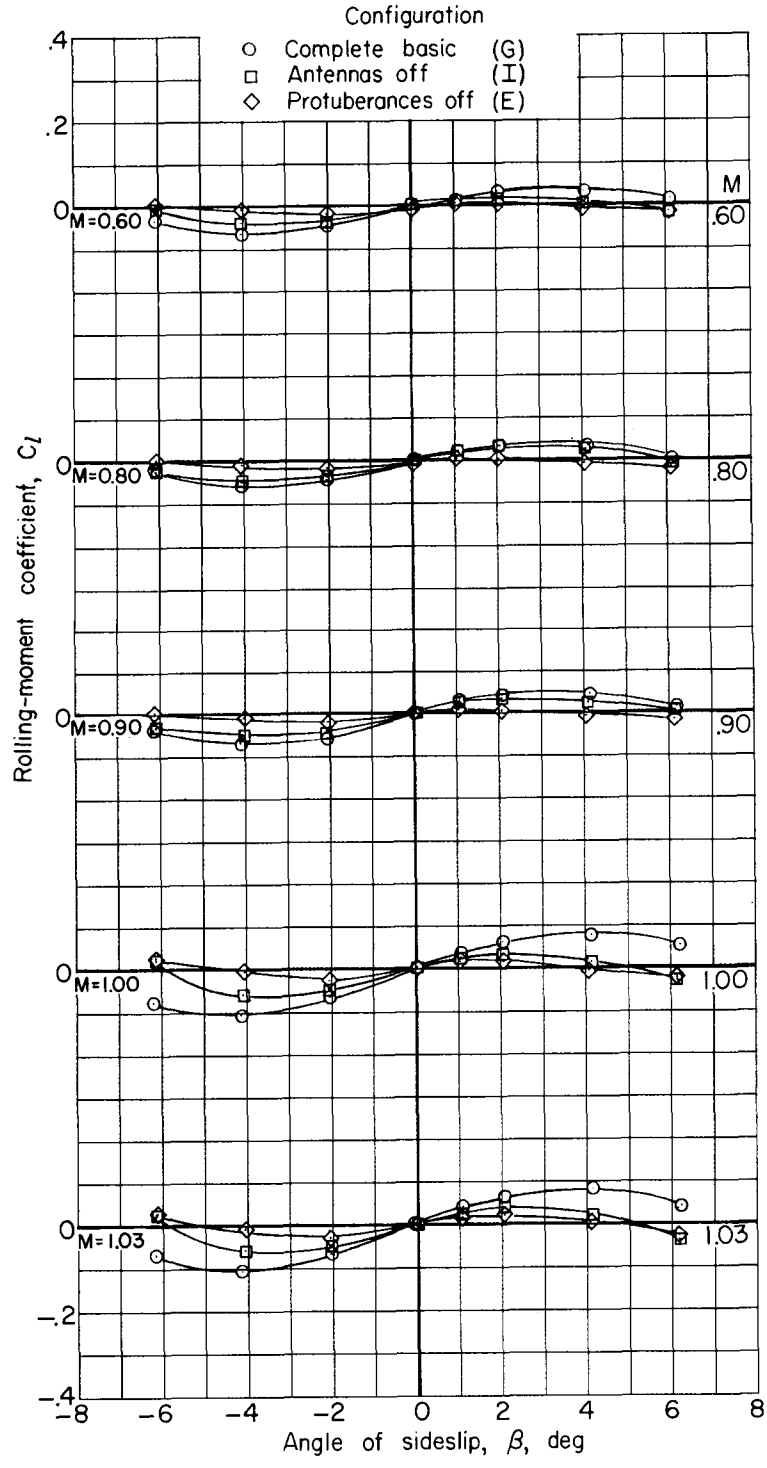

(b) $\alpha = 5^{\circ}$; configurations E, G, and I.

Figure 9.- Concluded.

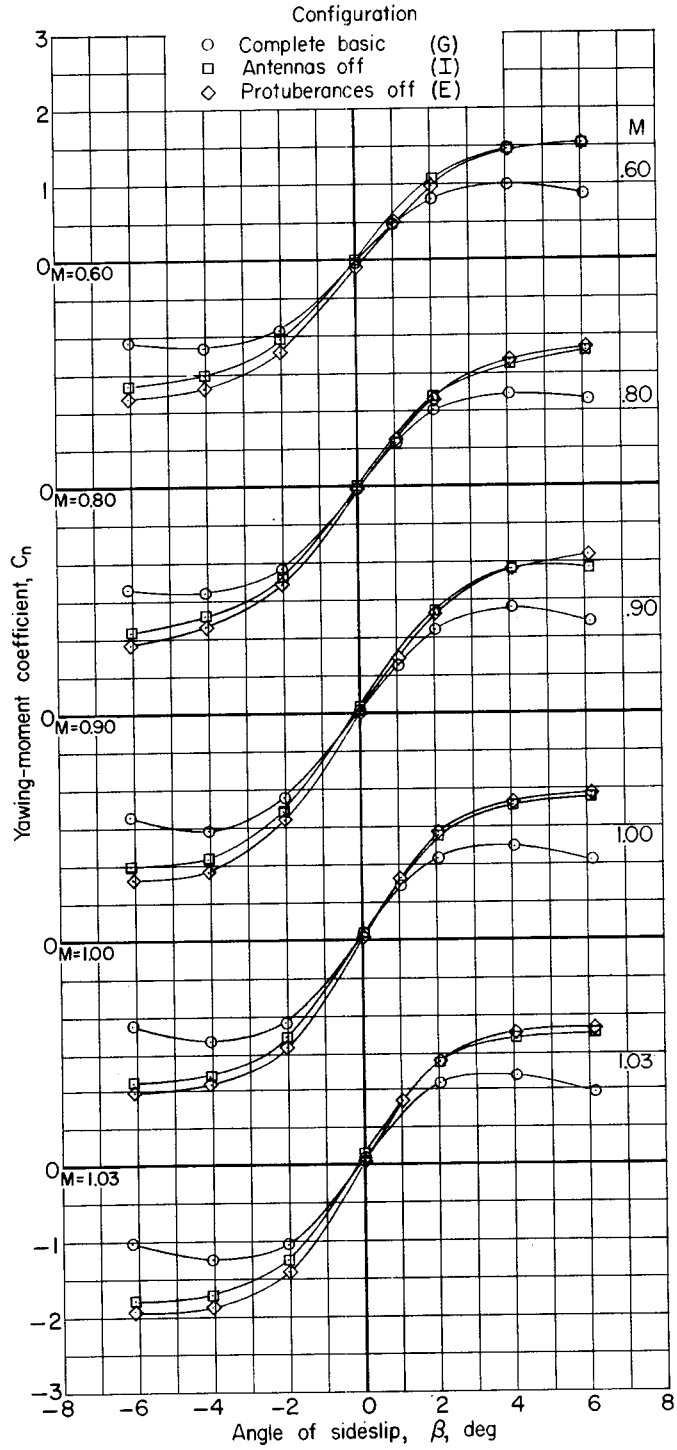

(a) $\alpha = 0^{o}$; configurations E, G, and I.

Figure 10.- Variation with angle of sideslip of yawing-moment characteristics.

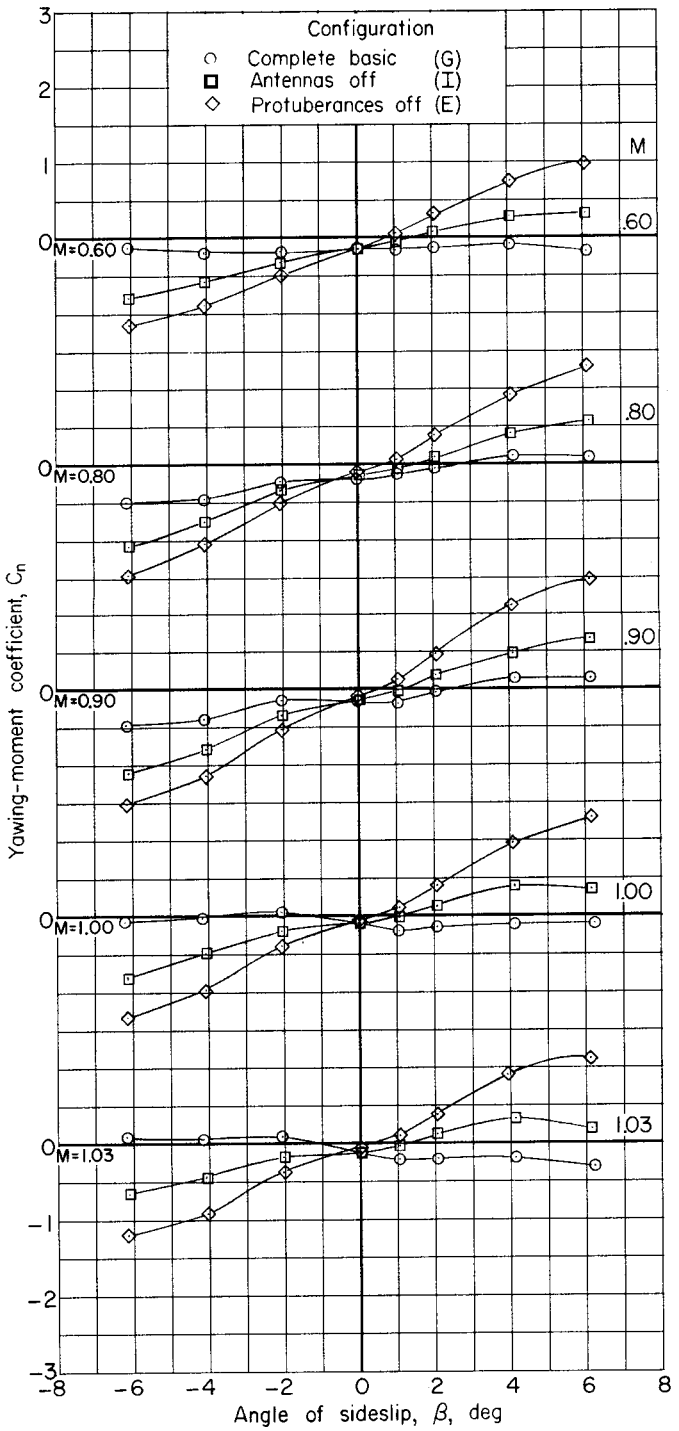

(b) $\alpha = 5^{\circ}$; configurations E, G, and I.

Figure 10.- Concluded.

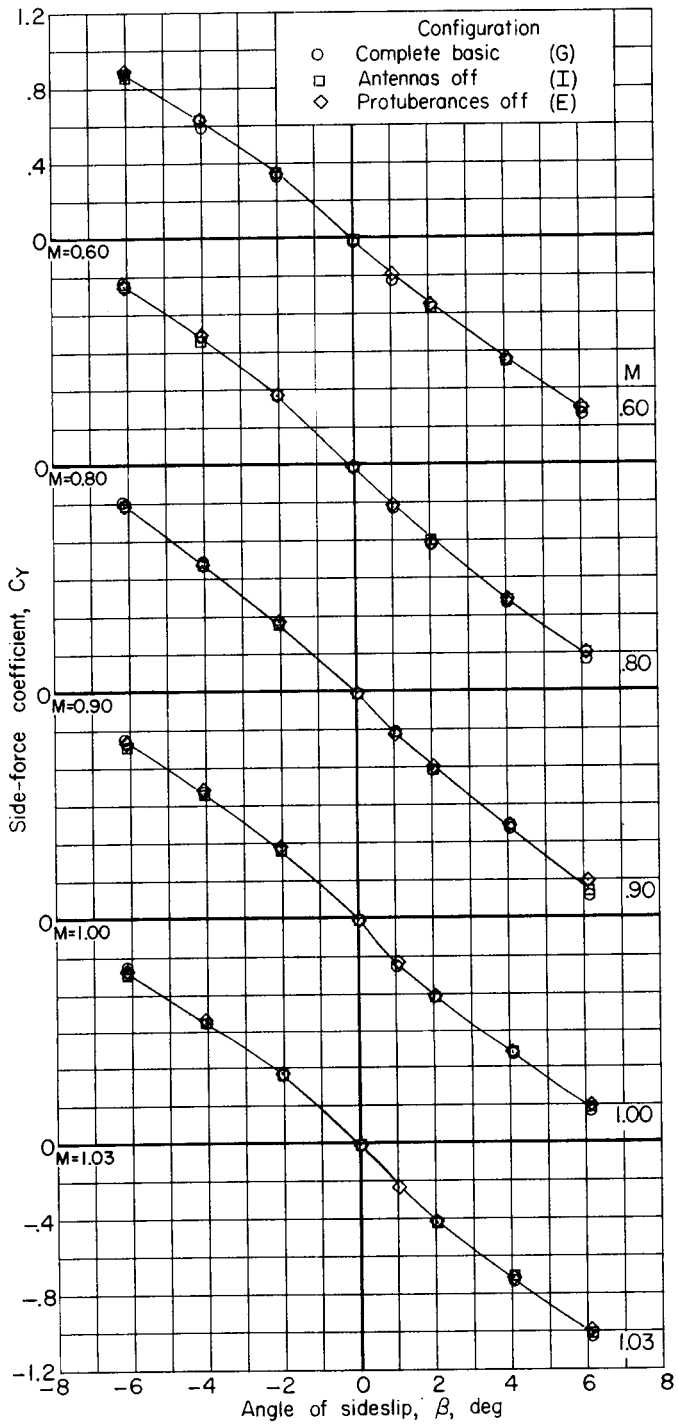

(a) $\alpha = 0^{\circ}$; configurations E, G, and I.

Figure 11.- Variation with angle of sideslip of side-force characteristics.

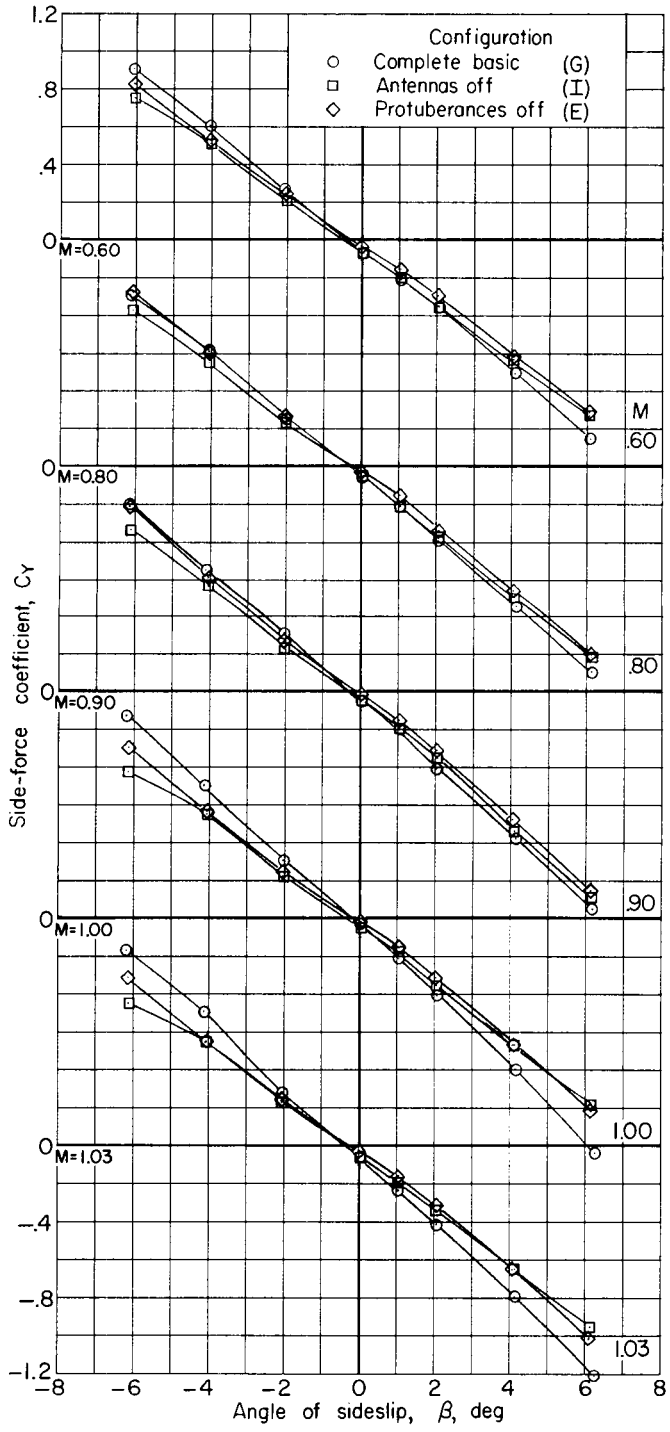

(b) $\alpha = 5^{\circ}$; configurations E, G, and I.

Figure 11.- Concluded.

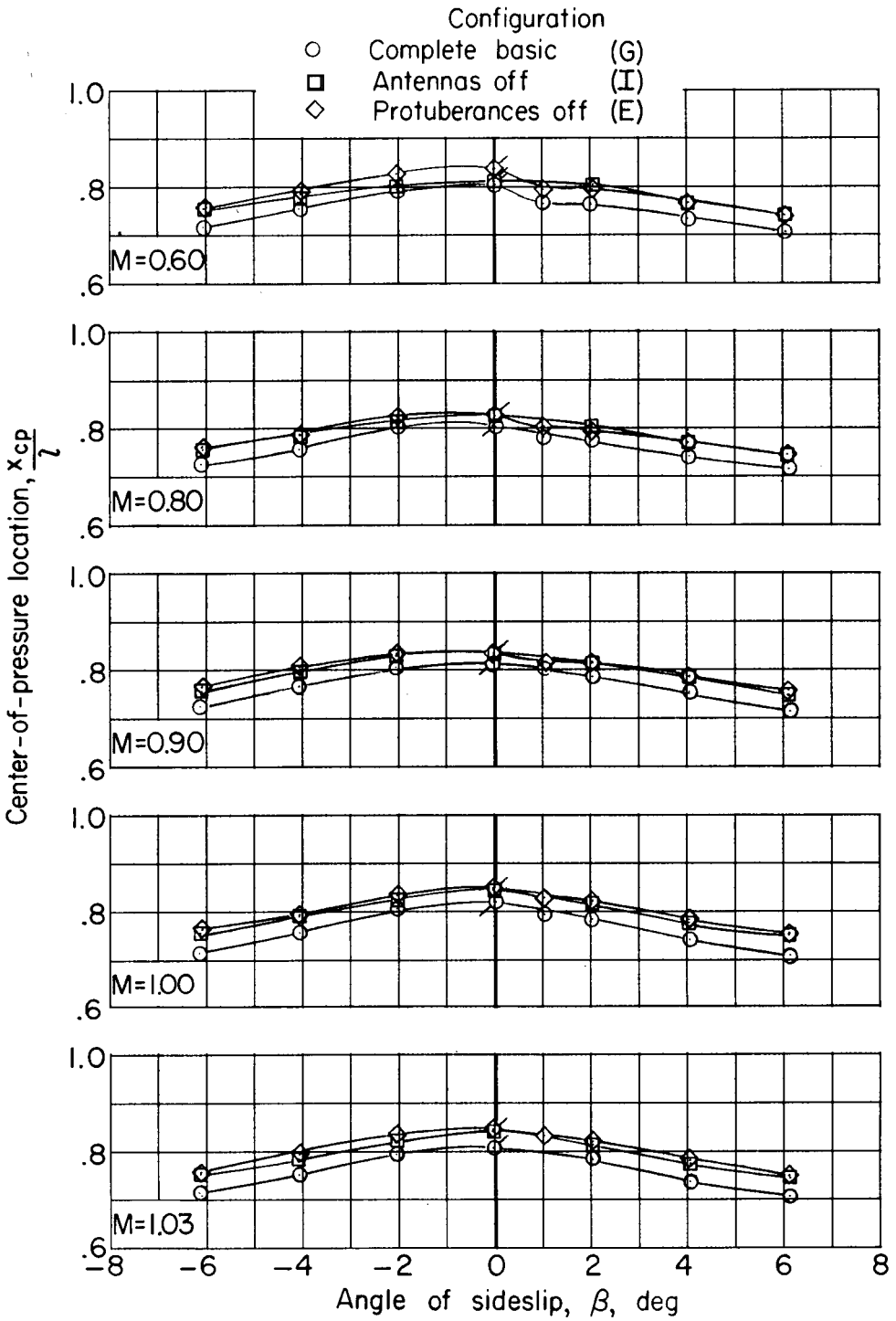

(a) $\alpha = 0^{\circ}$; configurations E, G, and I.

Figure 12.- Variation with angle of sideslip of directional center-of-pressure characteristics.

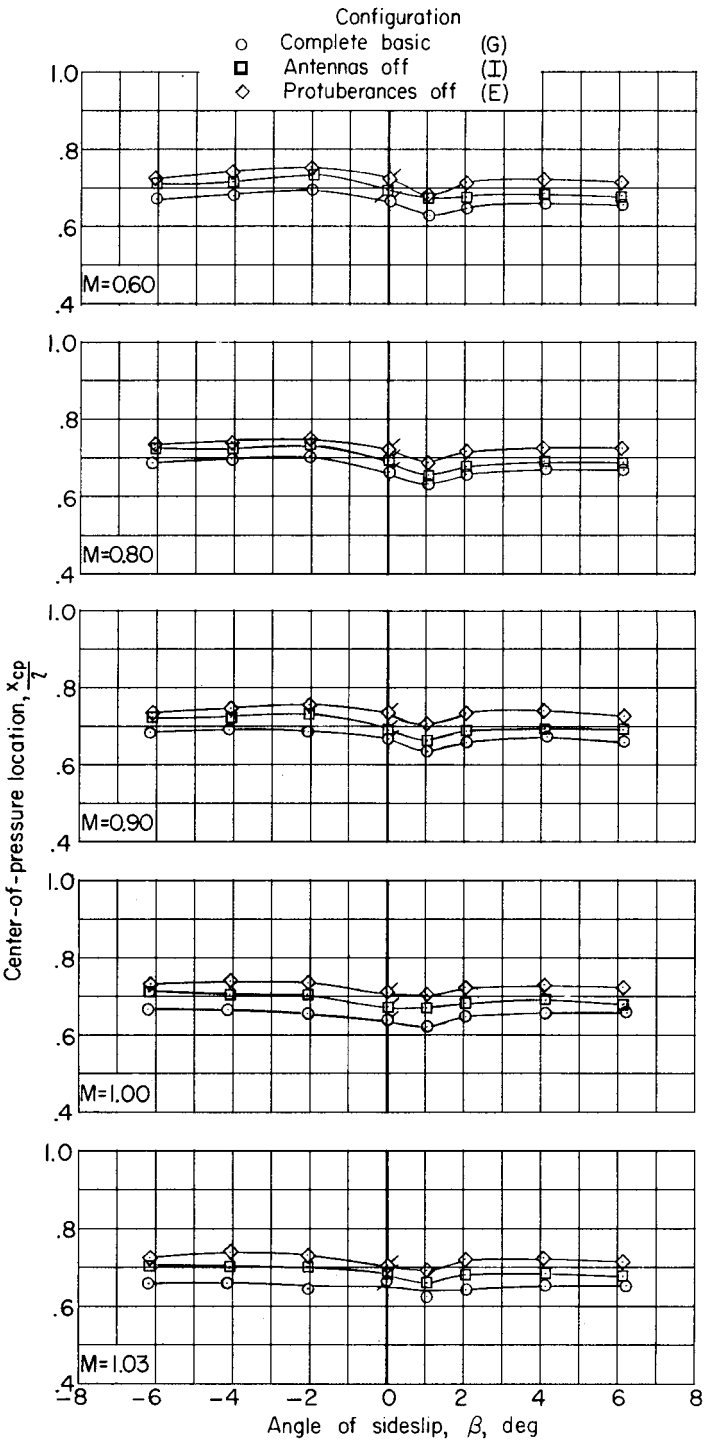

(b) $\alpha = 5^{\circ}$; configurations E, G, and I.

Figure 12.- Concluded.

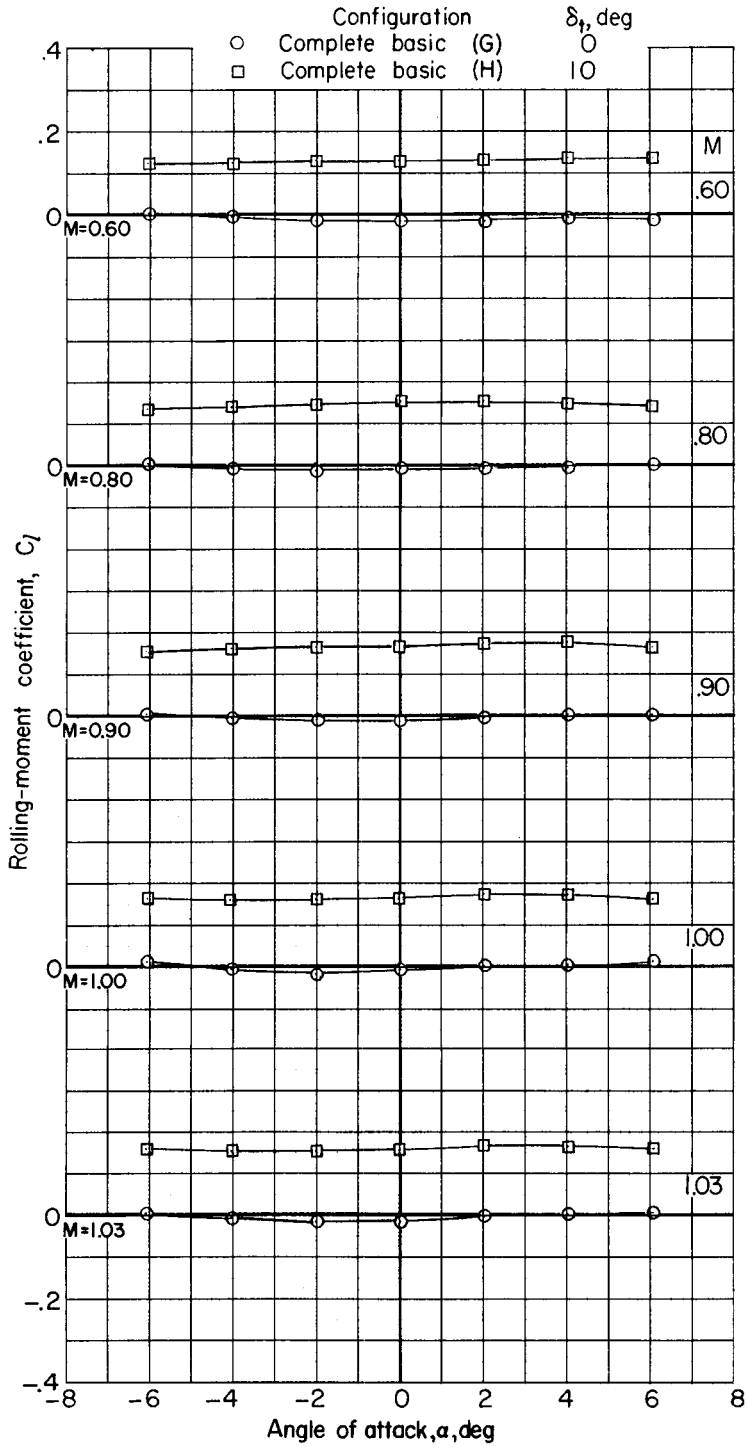

Figure 13.- Effects of tip-control deflection on rolling-moment characteristics.